Journal of African Earth Sciences 137 (2018) 69–90

Contents lists available at ScienceDirect

Journal of African Earth Sciences

journal homepage: www.elsevier.com/locate/jafrearsci

Paleoenvironments, $\delta^{13}C$ and $\delta^{18}O$ signatures in the Neoproterozoic carbonates of the Comba Basin, Republic of Congo: Implications for regional correlations and Marinoan event

Alain Préat [a, *], Franck Delpomdor [a, b], Anna Perla Ackouala Mfere [a, c], Yannick Callec [d]

[a] University of Brussels, Department of Earth Sciences and Environmental Sciences, 50 av. FD Roosevelt, B-1050, Brussels, Belgium
[b] Illinois State Geological Survey, University of Illinois, 650 Peabody Dr, US-61820, Champaign, IL, USA
[c] Université Marien Ngouabi, Département de Géologie, BP69, Brazzaville, People's Republic of Congo
[d] Bureau de Recherches Géologiques et Minières, 3 av. Claude Guillemin, BP 36009, F-45060 Orléans, Cedex2, France

ARTICLE INFO

Article history:
Received 19 October 2016
Received in revised form
10 August 2017
Accepted 1 September 2017
Available online 13 September 2017

Keywords:
Neoproterozoic
Schisto-Calcaire Group
Microfacies analysis
Isotope chemostratigraphy ($\delta^{18}O$ and $\delta^{13}C$)

ABSTRACT

The Ediacaran Schisto-Calcaire Group is a ~1300 m-thick succession belonging to the West Congo Supergroup in Central Africa. In the Comba Basin, it consists of three carbonate-dominated units defined as formations (SCI to SCIII) that are unconformably overlain by clastic deposits (Mpioka Group) interpreted as a molassic formation associated with the Panafrican Orogen. The underlying Upper Tillite and Cap Carbonate (SCI_a) units, considered as markers of the Snowball Earth event were studied in three sections. We investigated the carbonates of the Schisto-Calcaire Group by defining new microfacies (MF1-MF7) and we performed C and O isotopic analyses in order to constraint the depositional and diagenetic events directly after the Marinoan interval. Stratigraphic variations of the stable isotopes are important in the series with lighter $\delta^{18}O$ values (>1.5‰) than those of the Neoproterozoic ocean in the SCI_c unit. According to regional stratigraphy a temperature effect can be dismissed and a freshwater surface layer is the origin of such negative $\delta^{18}O$ values in this unit. The negative $\delta^{13}C$ anomaly (−3.5‰ on average) of the Cap Carbonate is similarly to the $\delta^{18}O$ values (−6.4‰ on average) in the range of the marine domain during postglacial sea level rise. The sample suite as a whole (SCII and SCIII formations) displays heavier $\delta^{18}O$ and $\delta^{13}C$ than those of the lower part (SCI unit) of the Schisto-Calcaire Group. The comparison with the Lower Congo (Democratic Republic of Congo) and Nyanga (Gabon) basins shows that the meteoric flushing in SCI_c unit of the Schisto-Calcaire Group was regional and not local, and could be derived from a climatic evolution. Although an overall overprint is present, our isotopic relationships argue against overall diagenetic resetting of primary compositions and suggest that with careful examination combined with detailed petrographic analysis general depositional and diagenetic controls can be discerned in oxygen and carbon isotopic data in the Schisto-Calcaire Group.

1. Introduction

Neoproterozoic glaciogenic successions are locally reported around the Congo Craton (Cahen and Mortelmans, 1947; Cahen, 1954; Verbeek, 1970; Béchennec et al., 1981; Poidevin et al., 1981; Poidevin, 1985; Poidevin and Pin, 1986; Vicat and Vellutini, 1987; Master et al., 2005; Walemba and Master, 2005; Wendorff and Key, 2009; Tait et al., 2011; Arnaud et al., 2011; Delpomdor and Préat, 2015). One of these glaciations occurring during the Marinoan event is revealed by the deposition of the Upper Tillite and the Cap Carbonate (SCI_a) units of the Schisto-Calcaire Group. These two units together are traditionally considered like a relevant stratigraphic marker related to the catastrophic Snowball Earth-type climatic model (Kirschvink, 1992; Hoffman et al., 1998; Hoffman and Schrag, 2002; Hoffman and Li, 2009). Our paper examines 25 new sections from the Schisto-Calcaire Group in the Comba Basin (Fig. 1 and Table 1) belonging to the Late Neoproterozoic (West Congo Supergroup *sensu* Mickala et al., 2014, Affaton et al., 2015, Fig. 2) exposed in the western margin of the Congo Craton in the Republic of Congo (Alvarez and Maurin, 1991). Geochronological and palaeomagnetic data from the West Congo Supergroup are scant, and ages and paleolatidudinal constraints are

* Corresponding author.
E-mail address: apreat@ulb.ac.be (A. Préat).

https://doi.org/10.1016/j.jafrearsci.2017.09.002
1464-343X/

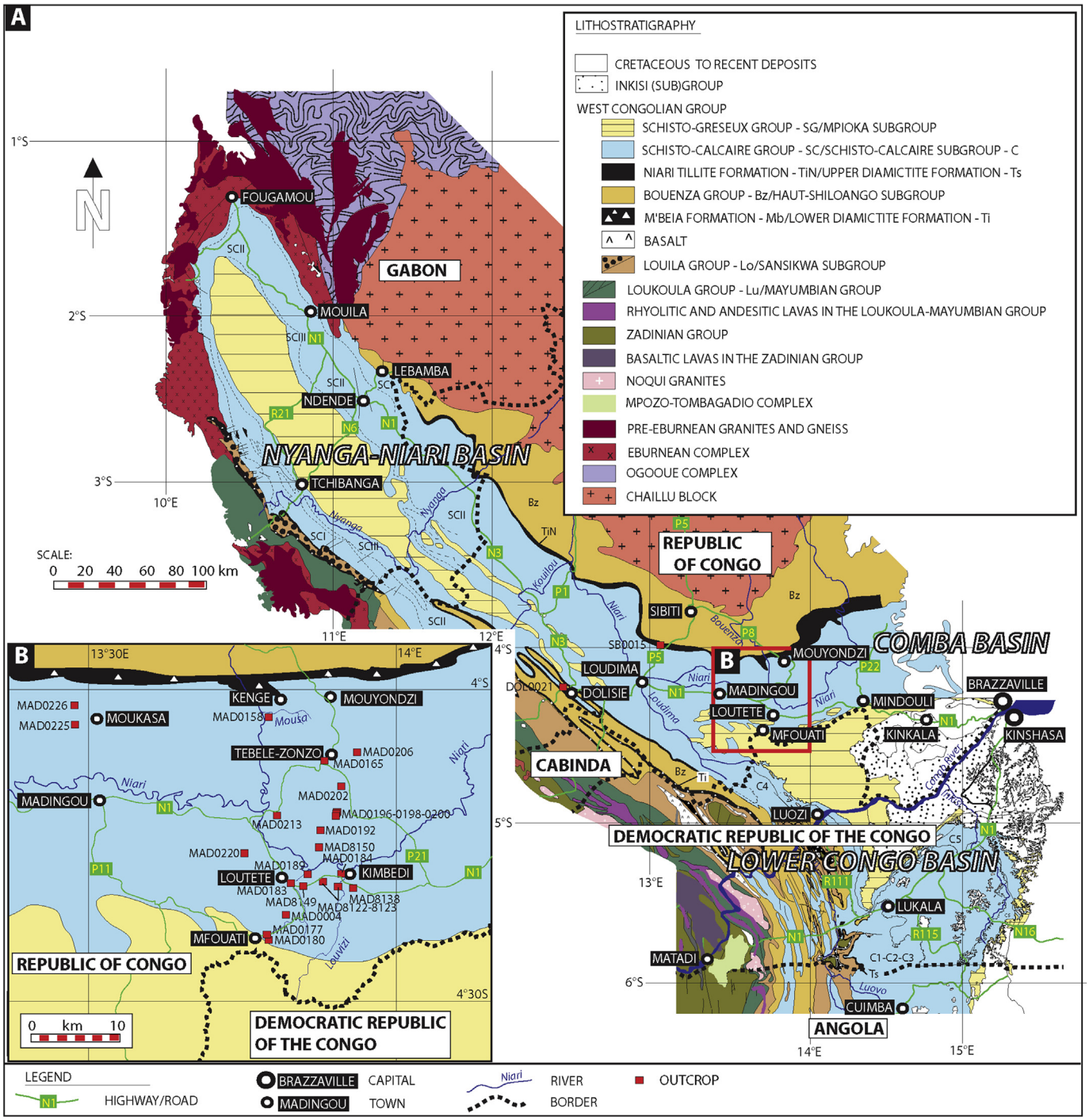

Fig. 1. General map of the West Congo area from SW Gabon to Angola, location of sections and outcrops (see Table 1), and main geological units.

derived indirectly by correlation (Evans, 2000; Poidevin, 2007; Straathof, 2011) or by dating which yielded an oldest age of 650 Ma *in* Alvarez et al. (1995) and Monié et al. (2012), and a youngest one 550 Ma *in* De Carvalho et al. (2000) and Frimmel et al. (2006). The aim of this paper is to interpret the sedimentological processes operating in the Neoproterozoic carbonates of the Comba Basin in relationship with the post-glacial Marinoan glaciation.

2. Methods

Numerous outcrops from 25 localities are selected for sampling, with plurimetric to decametric intervals in the ~800-1000 m-thick Schisto-Calcaire Group of the West Congo Supergroup in the Comba Basin (south of the Chaillu Massif, Fig. 1 and Table 1) of the Republic of Congo, located at ~100 km west of Brazzaville. Facies and diagenetic interpretations were corroborated by 255 thin sections. Microsamples for stable-isotope analysis were prepared as powders drilled from cut surfaces corresponding to areas that had been thin-sectioned. Samples were selected for isotopic analysis on the basis of fabric preservation, fineness of the grain and textural uniformity. Primary texture was the main selection criterion. Carbonate powders were reacted with 100% phosphoric acid (density >1.9, Wachter and Hayes, 1985) at 75 °C using a Kiel III online carbonate preparation line connected to a ThermoFinnigan 252

Table 1
Location of outcrop areas (coordinates X, Y) in the Comba Basin (from the data base of the BRGM). Abbreviations: MAD = Madingou, SB = Sibiti, DOL = Dolisie.

Sample	X (hddd.dddd°)	Y (hddd.dddd°)	Location Area
MAD8122	13.92118	−4.30612	National road n°1 - Loutété-Kimbédi
MAD8149	13.92274	−4.30705	National road n°1 - Loutété-Kimbédi
MAD8123	13.94423	−4.31346	National road n°1 - Loutété-Kimbédi
MAD8138	13.96760	−4.31618	National road n°1 - Loutété-Kimbédi
MAD8150	13.91325	−4.24641	SONOCC quarry - Loutété
MAD0158	13.83018	−4.02424	Kengué Village
MAD0165	13.92269	−4.09783	Zonzo Village
MAD0177	13.82757	−4.39883	Mfouati track
MAD0180	13.83103	−4.40389	Mfouati track
MAD0183	13.88492	−4.31301	Loutété River
MAD0184	13.95318	−4.29298	Kimbédi River
MAD0189	13.89573	−4.29413	Niari River
MAD0004	13.85892	−4.36135	Mfouati road
MAD0192	13.91659	−4.21776	Mindouri track
MAD0196	13.94169	−4.19123	Mousa River (Mindouri Village)
MAD0198	13.94090	−4.19400	Mousa River (Mindouri Village)
MAD0200	13.93886	−4.19440	Mousa River (Mindouri Village)
MAD0202	13.94931	−4.14365	Yamba track
MAD0206	13.97584	−4.08433	Mingenge Village
MAD0213	13.84521	−4.19274	Loutété track
MAD0220	13.79091	−4.25640	Kimbenza Village
MAD0225	13.51133	−4.03561	Djolo track
MAD0226	13.51161	−4.03437	Djolo track
SB0015	13.27774	−3.86727	Makoubi quarry
DOL0021	12.62579	−4.16955	Lissanga FORSPAK quarry

mass spectrometer. All values are reported in per mil relative to V-PDB by assigning a $\delta^{13}C$ value of +1.95‰ and a $\delta^{18}O$ value of −2.20‰ to NBS19. Reproducibility was checked by replicate analysis of laboratory standards and is better than ±0.04‰ (carbon) and 0.07‰ (oxygen) (1σ). The analyses were performed at the University of Erlangen (Prof. M. Joachimski). Samples were selected for isotopic analysis on the basis of fabric preservation as seen in thin section in transmitted light.

3. Geological framework

The West Congo Belt, exposed on 1300 km along the western margin of the Congo Craton, comprises several Neoproterozoic basins (Tait et al., 2011; Préat et al., 2011; Delpomdor and Préat, 2013, 2015) filled by volcano-sedimentary successions of the West Congo Supergroup (Fig. 2; Dadet, 1969; Lepersonne, 1974; Alvarez and Maurin, 1991; Tack et al., 2001; Frimmel et al., 2006; Thiéblemont et al., 2009; Delpomdor and Préat, 2015).

The Comba Basin is a ~150 km-long N60°E lithostratigraphic unit through perpendicular to the Nyanga-Niari and Lower Congo basins (Fig. 1; Alvarez and Maurin, 1991). Its tectono-sedimentary evolution was initiated in the Neoproterozoic (between 950 and 700 Ma *sensu* Alvarez and Maurin, 1991) and the through formed a NW-SE extension. The stratigraphy of this basin has been established by Scolari (1965) and Dadet (1969) and re-assessed by Alvarez and Maurin (1991). The Schisto-Calcaire Group, subdivided into four formations deposited in very shallow seas (SCI to SCIV; *sensu* Dadet, 1969. The stratigraphic position of the upper detrital unit (clayey and sandy), called SCIV Formation (Biboua series; Scolari, 1965), is still debatable. According to Mickala et al. (2014), this unit crosses the Schisto-Calcaire and the Mpioka (or 'Schisto-Grèseux' *sensu* Dadet, see Fig. 2) groups, or for others it constitutes the lower part of the Mpioka Group Charles et al., 2015a,b).

The basal SCI Formation is made of three members (a,b,c, Fig. 3). The SCI_a Member, overlying the Upper Tillite Formation (Fig. 2; Fig. 4A and B) with a slight unconformity, is a ~12 m regionally persistent thick unit of whitish and pinkish laminar dolomudstones representing the Cap Carbonate unit (Fig. 4C–F). The SCI_b Member about 300 m thick, is composed of finely laminated pink dolomitic claystones, red siltites with fine-grained sandstones, sometimes with hummocky cross stratification towards the top (Fig. 4H and I). The SCI_c Member consists of ~75 m–~90 m (Dadet, 1969) medium-bedded to massive stromatolitic dolobindstones and medium-bedded grey or cream-coloured oolitic dolopackstones/dolograinstones with angular and rounded millimeter/centimeter-sized intraclasts (breccias) and fenestral evaporitic dolomudstones and dolowackestones (Fig. 5A–F).

Overlying the SCI Formation, the SCII (~200-440 m-thick) and SCIII (~180 m thick) formations poorly outcrop with occasional terrigeneous intervals displaying wave ripples and desiccation cracks in the SCII (Fig. 5G) and abundant silicified stromatolites with some thin evaporitic levels in the SCIII (Fig. 5H). The SCIV Formation corresponding to detrital shallow marine to continental deposits (Scolari, 1965; Dadet, 1969; Alvarez, 1992; Charles et al., 2015a) is not studied here.

4. Depositional environments

4.1. Regional stratigraphic overview

The 'Schisto-Calcaire cycle' comprises a transgressive marl zone, a condensed dolomite section (SCI_a) which records a high sea level stand with a terrigeneous-carbonate ramp (SCI_b) and a carbonate barrier (SCI_c) prograding SW-NE towards the aulacogen (Alvarez and Maurin, 1991; Alvarez, 1995). Between the Comba and Nyanga-Niari basins, submarine dunes and infratidal giant stromatolites (Bertrand-Sarfati and Vicat, 1987; Trompette and Boudzoumou, 1988) overlain by oncolitic dolomites were formed in the SCI_c Member. Laterally, an evaporitic dolomitic lagoon is present in the Nyanga-Niari Basin and in the western part of the Comba Basin. It was bordered by an oolitic shoal preceding a deepening of the internal shelf towards the aulacogen. In the nearshore zone, laminated 'algal' deposits were associated to a tidal flat mixed with evaporites. Alvarez (1995) concluded that these basins correspond to internal shelf deposits isolated from the open marine environments by an oolitic and a stromatolitic continuous

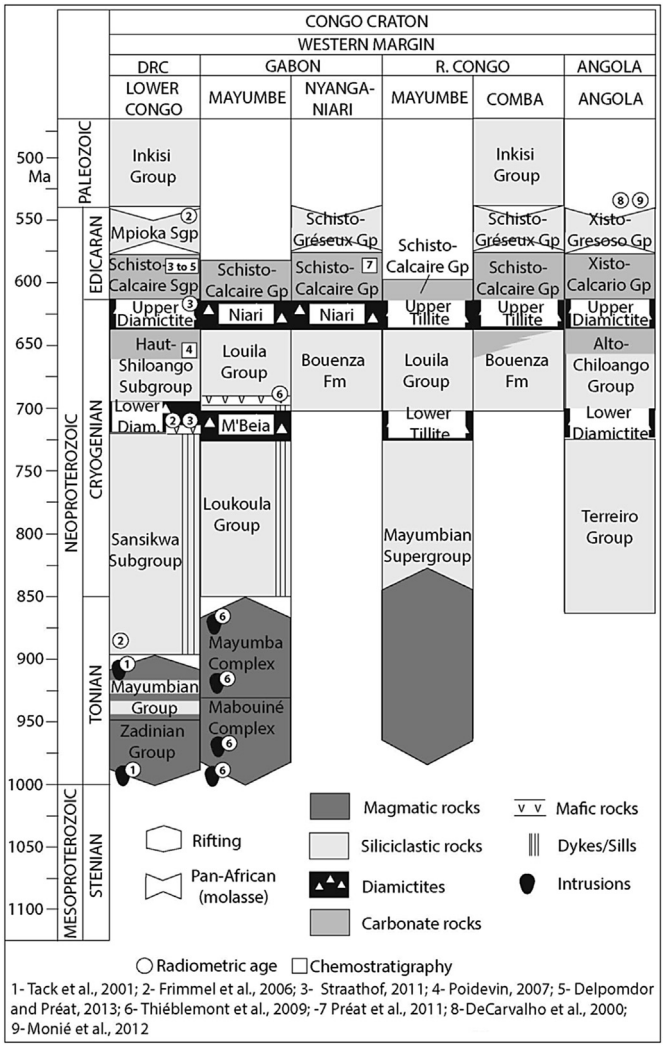

Fig. 2. Stratigraphic logs of Neoproterozoic sequences from the western margin of the Congo Craton. Correlations based on Sr isotopic data, radiometric age constraints and revised lithological relationships. References in bibliography.

barrier. Similar facies, environments and conclusions in coeval sedimentation of the Lower Congo region in the Democratic Republic of Congo (DRC) have been stated by Frimmel et al. (2006), Delpomdor (2007), Delpomdor and Préat (2013, 2015), Delpomdor et al. (2015, 2016), Cailteux et al. (2015).

4.2. Field observations

The most interesting and complete sections concern the SCI Formation and particularly the SCI_a (pink dolostones) and SCI_c (oolites, stromatolites, pre-evaporites) members (Fig. 3). The former ones are those of Kengué (samples cb93-112), Makoubi (samples cb229-248), the latter ones are those of Loutété ('SONOCC' quarry, samples cb34-92) and Tebele-Zonzo (samples cb116-149) (see Table 1 for location of the outcrops). All other samples relate to more discontinuous outcrops along rivers, roads or excavations. They cover the entire Schisto-Calcaire unit and some samples are taken from the underlying clastic Bouenza Formation (one sample, cb227) and the Upper Tillite (samples cb205/206/225/226) unit (Table 1).

4.2.1. The SCI Formation

The pink dolostone unit (SCI_a) is exposed at Kengué (MAD0158), Makoubi (SB0015) and along the Mousa River (MAD0198). In Kengué, the series is 10.6 m thick, and is overlain by thick red siltites of the SCI_b Member. In the Makoubi quarry, the SCI_a unit is 12.7 m thick, overlies the Upper Tillite and is overlain by SCI_b red carbonate siltites displaying hummocky cross stratification. In both sections the dolostones are pinkish, pale grey to white, thinly laminated with slightly wavy and discrete oblique stratification and reactivation surfaces. Pyrite is rarely observed in the two sections and two levels of greenish carbonate claystones (5 and 10 cm thick respectively) are present in the upper part of the Makoubi section. Greenish clayey diastems are also observed in few beds in the upper part of the Makoubi section with rare erosional gutters. Typical laminated dolostones show a peloidal fabric with smooth flat laminations and tiny fenestrae (Fig. 6A–D) The dolostone unit, overlying the Upper Tillite with a clayey sandy matrix at the contact, displays over 1 m megaripple structures with medium-angle (~30°) cross stratified laminae (Fig. 4D) already observed in homologous stratigraphic levels in Australia, Brazil, Canada, Namibia and Svalbard (references *in* Allen and Hoffman, 2005). This structure has also been reported in coeval levels in SW Gabon by Préat et al. (2011). In the Makoubi quarry, this structure appears to be limited and no '3D' geometry can be inferred due to limited condition of exposure. The upper part of the SCI_a unit is still well-bedded and contains large and soft ondulations with plurimetric wavelengths ensuring a progressive transition with the overlying member. Along the Mousa River (MAD0198), the Cap Carbonate unit overlies a 3–4 m thick cross-stratified feldspathic sandstone lying above the Upper Tillite.

The SCI_b Member, about 300 m thick, consists of red siltites and reddish to greyish carbonate siltites. It has been observed in several outcrops along roads and rivers and is transitional with the SCI_a unit (Makoubi section). In a few sections, the SCI_b series consists of coarsening- and thickening-upward plurimetric to decametric sequences (Fig. 4G) with small-sized erosional gutters (Fig. 4I), centimetric clayey intraclasts in the laminar lower part and hummocky cross stratification in the massive upper part (Fig. 4H). The best exposed sequences crop out in Kengué and Makoubi sections. This unit has not been examined in detail as it crops out rather poorly in the Comba Basin.

The SCI_c series, about 50–90 m thick, is well-bedded (pluricentimetric to metric beds) and consists on the field of four major facies of (i) light grey flat laminae (Fig. 5A), sometimes slumped, with domal LLH stromatolites (Lateral Linked Hemispheroidal *sensu* Logan et al., 1964) and/or 'giant' stromatolitic cone-shaped bioherms (up to 2 m heigh, 4 m wide, 6 m long, Fig. 5F) separated by narrow inter-reef areas representing erosional gutters filled with stromatoclastic dolopackstones (stromatoclasts are loosely packed, randomly to erectly orientated following fans and bundles, Fig. 5E); (ii) greyish to slightly pinkish intraclastic, 'filamentous' and ooid dolopackstones and dolograinstones, sometimes with low-angle planar lamination, nested small-scale cross-stratification, current ripple cross-lamination, which include an oomoldic porosity (Fig. 5C); (iii) greyish to darkish poorly sorted brecciated dolowackestones and dolopackstones (Fig. 5B); and (iv) fine-grained purplish and yellowish laminar or slightly undulating homogeneous dolomudstones. Facies (iii) is the thickest, the more massive and contains numerous well-expressed stylolites.

Evidence of lateral variation of the ooid bars is present in the ZONZO section (MAD0165). This section, overlying the red siltites of the SCI_b Member, contains in its lower part LLH stromatolites (Logan et al., 1964) and very large domal and cone-shaped 'reefal' stromatolites in its upper part.

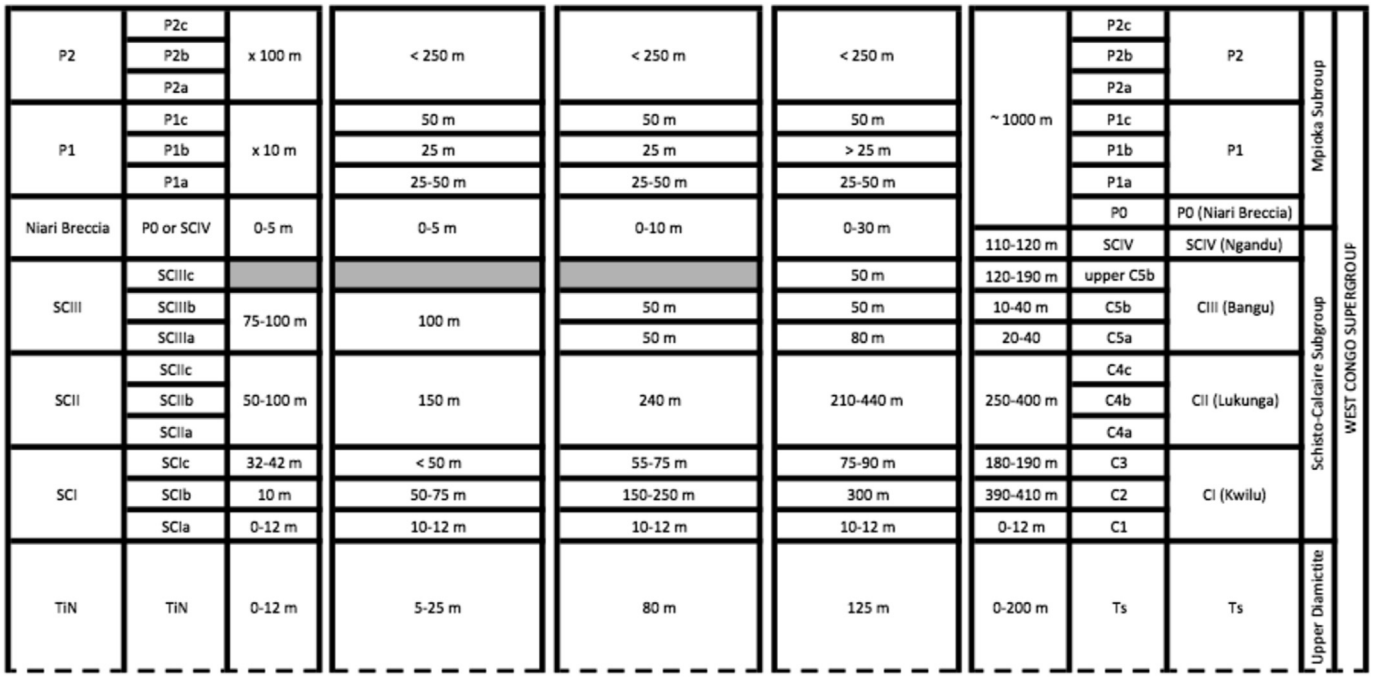

Fig. 3. Stratigraphic correlations of the different units (formations) in the Schisto-Calcaire Group in the Nyanga-Niari (Gabon, Prian et al., 2009; Thiéblemont et al., 2009), Lower Congo (DRC) and Comba (Republic of the Congo) basins (Dadet, 1969; Cailteux et al., 2015; Charles et al., 2015a,b; Delpomdor and Préat, 2015; Delpomdor et al., 2015). Mainly based on facies associations.

4.2.2. The SCII Formation

The SCII Formation (~200–440 m thick, Fig. 3) does not crop well and is represented in its lower part by reddish silty micaceous shales ($SCII_a$) overlain by well-bedded blue greyish and slightly reddish dolomudstones and dolowackestones with rare current-ripple cross-lamination ($SCII_b$ and $SCII_c$). The facies is sometimes brecciated (collapse breccia with angular intraclasts up to 7 cm long), and contains ooids and cherty interbeds (up to 5 cm thick). They show occasionally millimetric to centimetric fans of sulphate rods and needles (gypsum) and rare columnar stromatolitic levels (SH or hemispheroids *sensu* Logan et al., 1964).

4.2.3. The SCIII Formation

The SCIII Formation (~180 m thick, Fig. 3) present on the top of most of the hills as a result of its strong silicification consists of well-bedded stromatolitic dolobindstones and doloframestones, laminar microbial bindstones, marly dolomudstones/wackestones and evaporites (Fig. 5H) with thin enterolithic whitish levels and thick collapse brecciated units.

4.2.4. Remarks

Much of our work is concentrated on the best outcrops of the SCI Formation, the outcrops of the SCII and SCIII formations being too scattered or too silicified (for the latter). Meanwhile the three formations have been sampled and will be documented in the study.

We collected also a few samples in the underlying Upper Tillite (80–125 m thick *in* Scolari, 1965; Dadet, 1969) and in the upper part of Bouenza series 'Bz_4', (10–80 m thick, *in* Scolari, 1965; Dadet, 1969) (Fig. 3). The Bouenza series is predominantly siliciclastic with four units (Bz_1 to Bz_4). Rare thin beds of oolitic dolostone are observed locally in its upper part, they are generally eroded by the Upper Tillite. Rare clasts of these beds have been included in the overlying polygenic Upper Tillite, which exhibits a reddish clayey sandy matrix.

4.3. Microfacies and paleoenvironmental interpretation

We recognize seven main regionally correlative environments and associated microfacies (MF1 to MF7, Figs. 8 and 9) whose succession from 1 to 7 records the evolution of a marine shelf submitted to evaporation, with low energy outer-ramp environments (MF1-2), ooid shoal and biohermal mid-ramp (MF3-4-5), and restricted tide-dominated lagoonal inner-ramp settings submitted to evaporation (MF6-7). The ramp margin is characterized by thick stacks of ooid dolopackstones/dolograinstones (shoals) and stromatolitic bioherms, particularly in the SCI_c Formation (Kengué outcrop and SONOCC quarry, the liholog of the latter is illustrated in Fig. 10 as a typical example of the SCI_c succession).

The rock record of subenvironments is combined into larger genetically linked sets of subfacies (i.e., microfacies) defined as facies assemblages forming the fundamental building blocks of cycles or sequences (Clough and Goldhammer, 2000).

The microfacies are summarized and interpreted as follows (Figs. 8 and 11 for the paragenetic sequence):

4.3.1. Deep open marine environment

4.3.1.1. Microfacies 1 (MF1): deep subtidal mudstone. Light grey or purple homogeneous clayey dolomudstone, sometimes with millimeter-to centimeter-scale bedding-parallel characterized by black organic debris (30–100 μm) and clays (sericite). Pyrite is common, and consists of spheroids with diameters ranging between 5 and 30 μm. This microfacies is present in the SCI_c Member beneath and above giant stromatolitic cone-shaped 'reefs' and hummocky beds (see microfacies 2). It also occurs in the SCII Formation which does not crop well and exhibits rare current-ripple cross-lamination.

Environment: This microfacies represents deep subtidal outer ramp muds deposited by suspension settling beneath or near the storm wave base, probably tens of meters deep.

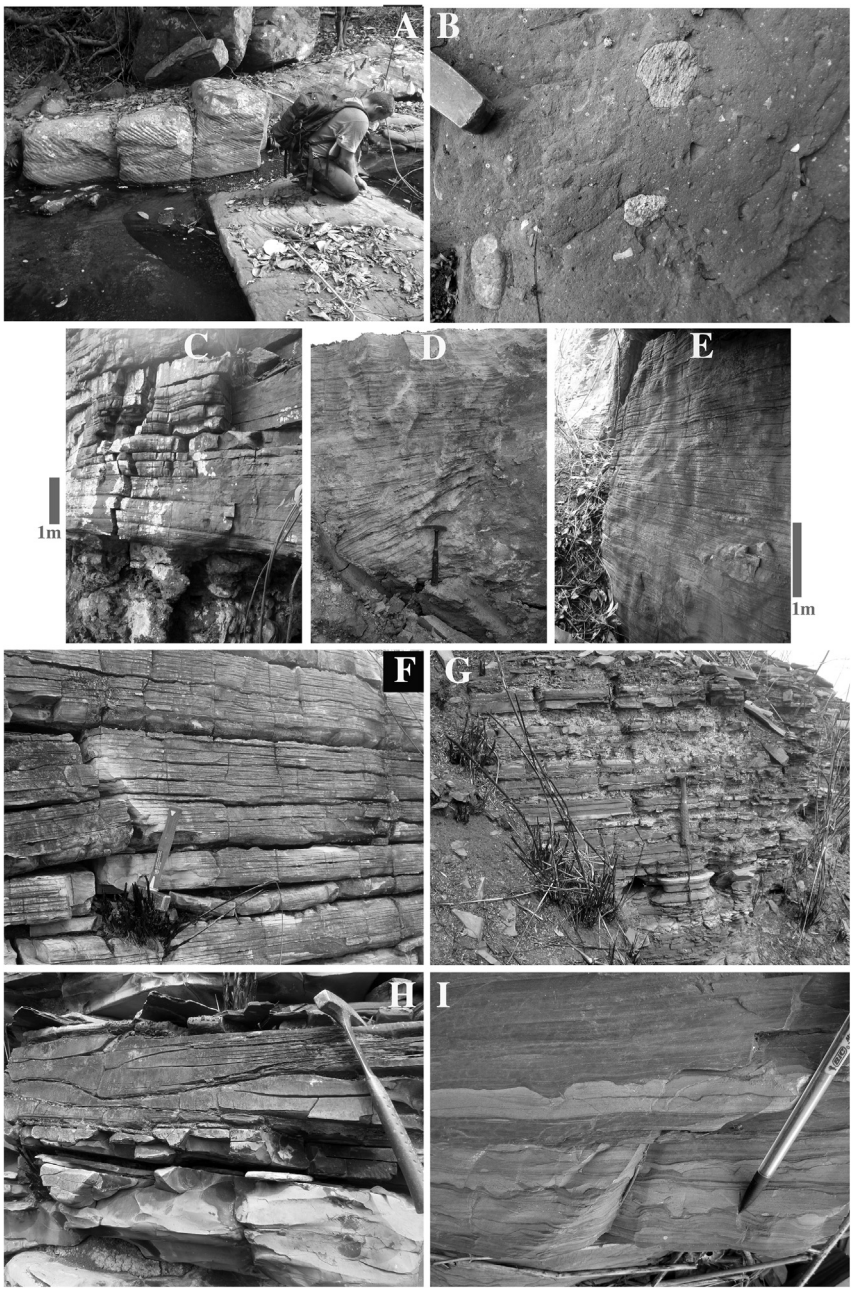

Fig. 4. (A–B) Cross-laminated feldspathic sandstone (A) interstratified in the Upper Tillite (B) showing curved bases and a sharp erosive top. The sandstone has a thickness of 3 m. The Upper Tillite (B) consists of a pebbly mudstone with poorly sorted clasts of mixed composition in a fine-grained clayey reddish/purplish matrix. Rare carbonate clasts (oolites, samples cb205 and cb206) are present and have been collected for C and O isotopic analyses. Part of the hammer on the upper left corner for scale. Upper Tillite, respectively photos 0963/2012/ap and 0994/2012/ap, MAD0196. (C) Sharp contact between the Upper Tillite (TiN, Fig. 3 in text, lower part of the picture) and the overlying laminated Cap Carbonates (SCIa, base of the Schisto-Calcaire Group) along the Mousa River, near the Mindouri village, photo 0999/2012/ap, MAD0198. (D) Lower part of the Cap Carbonates, 1 m above the Upper Tillite. The lower part of the Cap Carbonate unit displays over 1 m megaripple structures with medium-angle (~30°) cross stratified laminae, the laminae become sub-horizontal in the upper part, SCIa, base of the Schisto-Calcaire Group, photo 0273/2012-ap, SB0015 (Makoubi quarry). (E–F) Well-bedded and thinly laminated Cap Carbonate unit, the section is 6 m-thick (E), SCIa, base of the Schisto-Calcaire Group, respectively photos 0568/2012/ap and 0564/2012/ap, Near MAD0158 (G–H) Interbedded red siltstones and clayey siltstones, sligltly dolomitic (G) with hummocky cross-stratification showing parallel and medium-scale wavy lamination and strong erosive contacts (H). Hammer for the scale. SCIb, lower part of the Schisto-Calcaire Group, respectively photos 0675/2012/ap and 0671/2012/ap, MAD0158 (I) Laminated well-bedded red and pinkish siltites with small-scale gutter casts (scour and fill) and lower part of SCIb overlying the Cap Carbonate unit, lower part of the Schisto-Calcaire Group, photo 0333/2102/ap, SB0015 (Makoubi quarry).

4.3.2. Shoaling complex and barrier-bar system

4.3.2.1. Microfacies 2a (MF2a): high-relief stromatolites. This microfacies embodies a variety of stromatolitic morphologies including cone-shaped or elongated, domal, columnar, undulatory. An up to 1.5 m-thick vertical succession of stromatolitic morphologies is common from cone-shaped to columnar and undulatory. The cone-shaped 'reefs' consist of dolobindstones or meter-scale bioherms dipping along N20° (Fig. 5F) separated by narrow inter-reef areas filled with stromatoclastic dolopackstones (Fig. 5E). The stromatoclasts form a slumped breccia occupying channel-like structures or gutters in the inter-reef areas. These clasts consist of light grey microbial dolobindstones (Fig. 5A), with smooth or slumped laminae and low domal columns (Fig. 5B). Sediment between bioherms consists of elongated stromatoclasts or

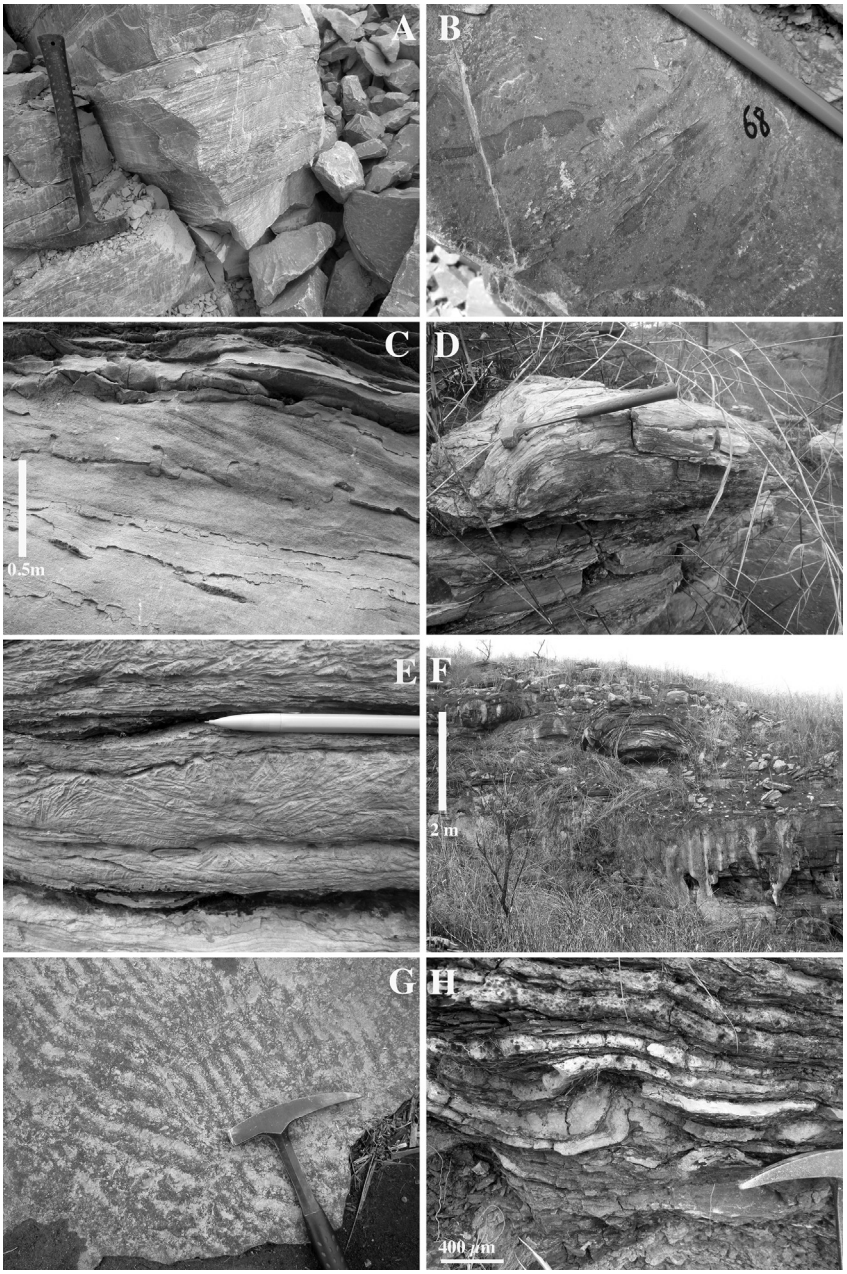

Fig. 5. (A-B-C) Medium-thick flat-laminated to slightly undulating dolomudstone (microbial mats) (A, hammer for scale), coarse-grained intraclastic and ooid dolograinstone showing cross-bedding (B, pen in upper right corner for scale, near sample cb68) and medium-grained oolitic dolograinstone with parallel and cross-lamination with medium angle erosional (reactivation) surface near the top (C), respectively, photos 0457/2012/ap, 0494//2012/ap, 0762/2012/ap, SCIc, lower part of the Schisto-Calcaire Group, MAD8150 (SONOCC quarry). (D-E-F) (D) Low-relief mound of a stromatolite overlying medium-thick flat laminated beds (microbial mats); (E) coarse-grained stromatoclasts showing a radial disposition and filling large subhorizontal gutters (pen for scale) between metric and plurimetric domal cone-shaped stromatolites (F), respectively photos 0715/2012/ap, 0712/2012/ap and 0099/2012/ap, SCIc, lower part of the Schisto-Calcaire Group, MAD0165 (ZONZO hill). (G) Plane view of sharp-crested, sinuous symmetrical ripples in a reddish dolomitic siltite, photo 0857/2012/ap, SCIIb middle part of the Schisto-Calcaire Group, MAD0183 (Loutété River). (H) Folded thin beds of evaporitic strata accumulated into folds of minor order leading to thickness variations of the strata, photo 0840/2012/ap, SCIII upper part of the Schisto-Calcaire Group, MAD0179.

calimicrobialite sandchip intraclasts forming centimetric radial bundles or stacked without particular orientation in a packstone texture. Bioherms are closely associated with hummocky cross-bedded (HCS) packstones/grainstones that are present beneath and above the stromatolite structures.

Environment: The vertical succession of stromatolitic forms results in a reduction in stromatolitic synoptic relief, recording a shallowing of water depth due to a relative sea level fall and/or upward stromatolitic growth (Hoffman, 1974). Giant cone-shaped stromatolites inhabited the subtidal outer ramp in deep channel environments submitted to storm-driven waves which produced the stromatoclasts while the wavy stromatolitic grew in moderate water depths in the mid ramp setting near the fair-weather wave base as there are locally interstratified and overlain by the cross-stratified oolitic grainstones of microfacies 2b (see below). The stromatolitic bioherms are interpreted to grow in the deep to shallow subtidal environment between or near linear tidal sand ridges composed of oolites.

4.3.2.2. Microfacies 2b (MF2b): subtidal sandy ooid shoal. This

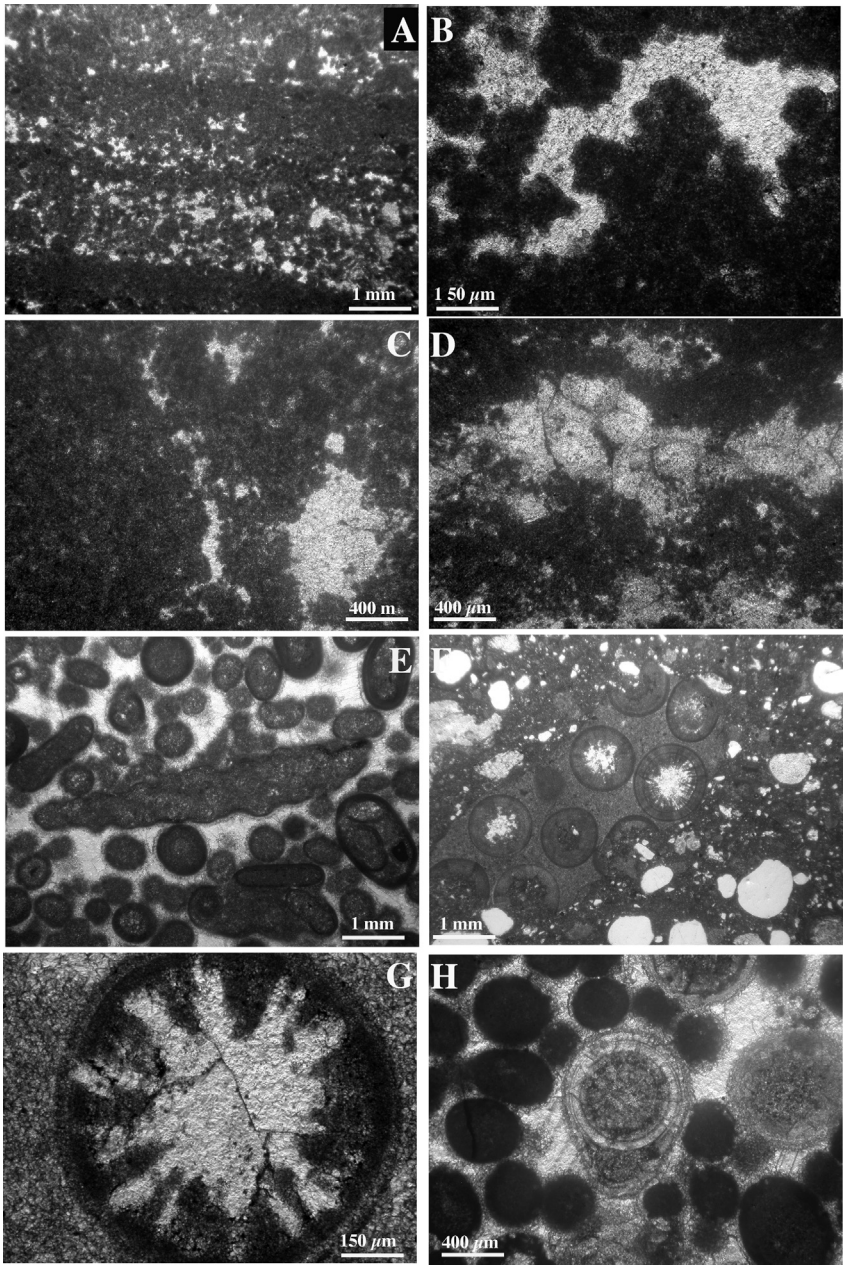

Fig. 6. (A–D) Typical laminated Cap Carbonate microfacies showing a peloidal dolomudstone-dolopackstone with a smooth flat lamination. In the peloid lamina a vertical trend of tiny fenestrae (C) is present and associated with irregular calcitic fenestrae (B) revealing a probable escape structure, respectively sample cb95, photo 0145/2013/ap, sample cb104, photo 097/2013/ap and sample cb96, photo 0152/2013/ap SCIa, lower part of the Schisto-Calcaire Group, MAD0158. (D) Same facies as previous pictures, with assembled yellowish calcitic tubes in the peloidal and fenestral laminae. They extent inside the laminae over a 3 mm distance, sample cb99, photo 0166/2013/ap SCIa, lower part of the Schisto-Calcaire Group, MAD0158. (E) Grainstone-rudstone with well sorted ooids and reworked ooidic grapestones. Cementation consists of a slightly greyish rather isopachous lamellar calcite with rare meniscus contacts and pendulant crystals and a coarse-grained granular white sparry calcite, sample cb81 photo 0020/2013/ap, SCIc, lower part of the Schisto-Calcaire Group, MAD8150 (SONOCC). (F–G) Ooid dolopackstone with sandy (millimetric) rounded quartz grains. Ooids consist partly of calcite replaced rosette-like sulphate crystals (see G), they are sometimes silicified, respectively sample cb28, photo 9343/2012/ap, SCII, middle part of the Schisto-Calcaire Group, MAD8123 and sample cb58, photo 9841/2013/ap, SCIc, lower part of the Schisto-Calcaire Group, MAD8150 (SONOCC quarry). (H) Ooid grainstone with pendulant or microstalactitic calcite beneath a partly recrystallized ooid, with fibrous and sparry calcite cements around the micritized ooids, sample cb85, photo 0076/2013/ap, SCIc, lower part of the Schisto-Calcaire Group, MAD8150 (SONOCC quarry).

microfacies consists of light grey ooid-pisoid intraclastic dolopackstone and dolograinstone characterized by a microconglomeratic texture. The matrix of the dolopackstone is sometimes peloidal and both facies contain abundant micritized grains. The micritic matrix is frequently microsparitized with greyish to whitish of equigranular calcite crystals delineating irregular patchs. Many of the grains have been micritized to varying degree, in some instances micritization has been so extensive that the original identity of the particles is lost. Elongated sandchip intraclasts (angular to subrounded), millimeter-sized to centimeter-sized, consist of ooid dolopackstone/dolograinstone, grapestone dolopackstone (Fig. 6E) and muddy facies. In the dolograinstones, the former isopachous intergranular fibrous cement (aragonite?) around the components is partly to totally replaced by a greyish equant to bladed calcite (5–15 μm) forming circumgranular thin crusts. The remaining porosity (often > 25%,

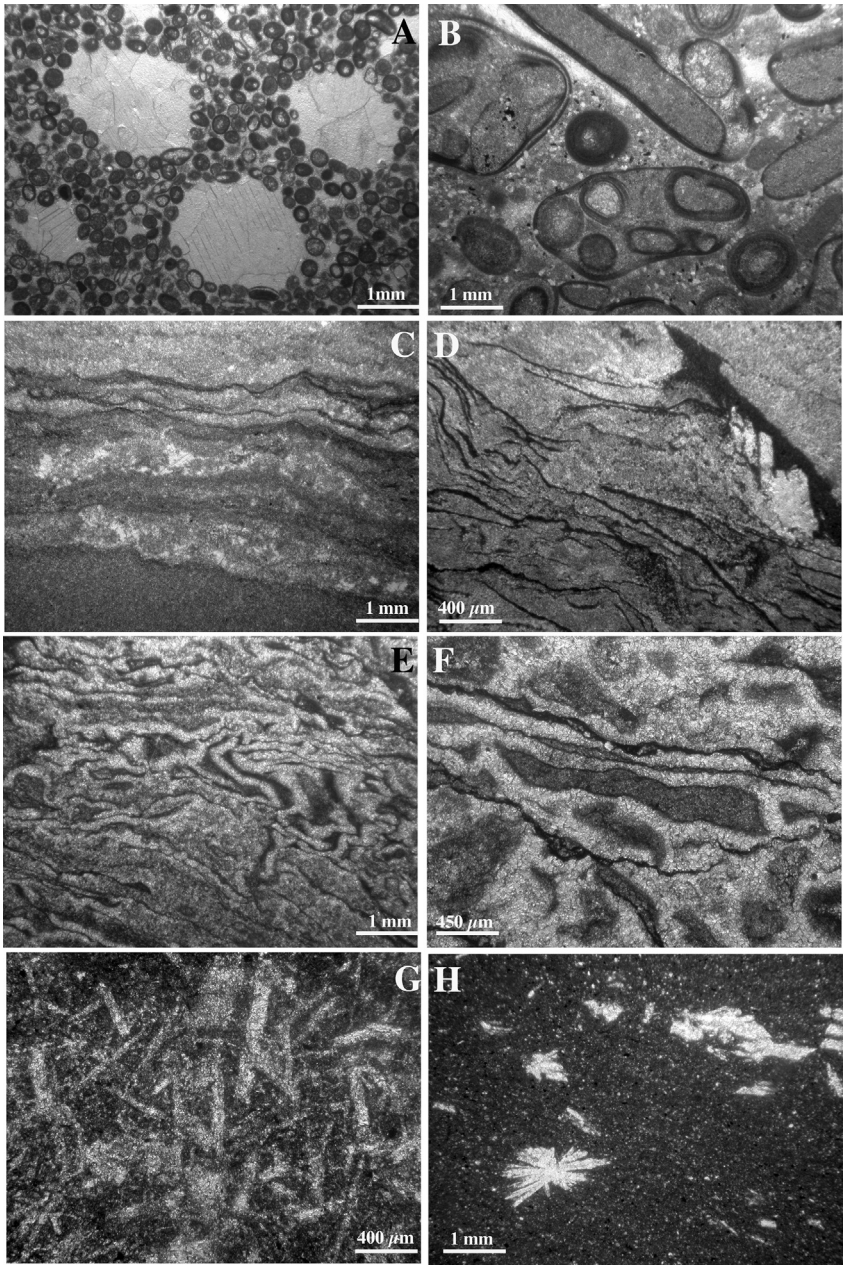

Fig. 7. (A) Oolitic grainstone with large ovoid to circular keystone vugs filled with a coarse-grained sparry calcite. Most of the oolites are micritized and partly dolomitized, sample cb99, photo 0099/2013/ap, SCIc, lower part of the Schisto-Calcaire Group, MAD8150 (SONOCC quarry). (B) Dolomicrosparitic packstone with micritized ooids and coarse-grained ooid intraclasts of the same facies. An oblique shelter cavity (umbrella) is located below a micritic intraclast and shows a partly vadose infilling by a peloidal muddy matrix, sample cb45, photo 9436/2012/ap, SCIc, lower part of the Schisto-Calcaire Group, MAD8150 (SONOCC quarry). (C) Dolomudstone consisting of the alternation of slightly deformed organic-rich micritic layers (dark) and dolomicrosparitized layers (whitish) with replaced sulphate crystals, sample cb149, photo 959/2013/ap, SCIc, lower part of the Schisto-Calcaire Group, MAD0165 (ZONZO) (D) Fine-grained dolomudstone (dark zones) and dolomicrosparite (whitish zones) with microenterolithes. The xenotopic dolomitic crystals are separated by discontinuous black thin veneers representing former microbial mats. Replaced large white sulphate crystals are present in the middle left side of the photo, sample cb17, photo 9238/2012/ap, SCII middle part of the Schisto-Calcaire Group, MAD8122. (E) Strongly deformed (with multiplication of primary thickness by folding related to former evaporites) fine-grained dolomicrosparite (white) in a former dolomudstone (dark), sample cb10, photo 9258/2012/ap, SCII middle part of the Schisto-Calcaire Group, MAD8122. (F) Partly replaced micrite facies with very thin microbial mats (darkish) by a fine-grained dolomicrosparite (whitish) isolating muddy patches (relics) resembling 'false intraclasts', sample cb24, photo 9307/2012/ap, SCII middle part of the Schisto-Calcaire Group, MAD8149. (G) Abundant laths, sometimes radiated, of replaced sulphate with anhydrite relics, sample cb92, photo 0122/2013/ap, SCIc, lower part of the Schisto-Calcaire Group, MAD8150 (top of SONOCC quarry). (H) Dolomudstone with rosettes and aggregates of laths and lenticular replaced sulphate crystals with anhydrite relics, sample cb174, photo 2055/2014/ap, SCII, middle part of the Schisto-Calcaire Group, MAD0184.

visual estimation) is filled by clear translucent white calcite crystals (up to 300 μm). The ooids and former sulphate minerals are commonly replaced by a large-sized granular dolomite, small-sized equant calcite and/or large white granular calcite from former radiated sulphates (Fig. 6F and G). Sometimes the ooids are dissolved, partially or totally, and cemented by two generations of calcitic cements, the first one is isopachous lamellar and is followed by a granular calcite in large crsytals. No or very weak mechanical grain compaction occurred, the cements are only rarely broken. Ooids (0.5–2 mm) are highly spherical, well sorted, have a well laminated and/or a radial cortex and, are sometimes polygenic (clusters of ooids) or asymmetric as a result of former pendent or

Microfacies	Fabric	Grain Types	Stratification	Origin
MF1	clayey dolomudstone	*organic debris, pyrite*	mm-cm laminae with hummocks (HCS)	*Deep subtidal outer ramp*
MF2a	giant cone-shaped stromatolites columnar, undulatory stromatolites dolo-bindstone/framestone	*peloids, stromatoclasts, bundles*	mm laminae with erosional gutters with hummocks (HCS)	*Subtidal bioherms, outer/mid ramp in deep channels*
MF2b	microconglomeratic dolo-packstone/grainstone	*ooids, pisoids, intraclasts, micritized grains sulphate pseudomorphs (rosettes)*	planar, asymmetrical ripples multiple cross-bedding	*Mid/inner ramp, sandy shoal, episodic vadose conditions*
MF3	dolo-packstone/grainstone/rudstone interstratified with dolowackestone	*as MF2b with abundant proto-oolites, abundant sulphate microcrsytals keystone vugs*	multiple cross-bedding	*Active crest of a shoal, common vadose conditions, inner ramp*
MF4	dolo-mudstone/wackestone/packstone	*peloids, grapestones, pyrite rare microbial intraclasts and ooids leached sulphate laths and rods*	laminar and non laminar	*Bankward edge of food tidal flat delta inner ramp*
MF5	dolo-packstone/grainstone interstratified with dolomudstone with desiccation mud-cracks	*peloids, intraclasts fans of sulphate crystals, pyrite*	laminoid fenestral, planar to undulatory	*Intertidal-supratidal channels temporary hypersaline conditions*
MF6	dolo-mudstone/microsparite with microtepee with monogenic breccia	*peloidal-alveolar grains, pyrite abundant sulphate pseudomorphs*	mm smooth flat laminae very low angle cross bedding	*Microbial marsh, backslope of levees evaporitic conditions*
MF7	dolo-mudstone/microsparite with enterolithic small nodules with slumps and small-scale folds and collapse breccia	*abundant sulphate pseudomorphs (laths, rosettes, aggregates, nodules)*	poorly stratified intense evaporitic deformation	*Littoral lagoon/sabkha*

Fig. 8. Neoproterozoic microfacies in the Comba Basin and their characteristics.

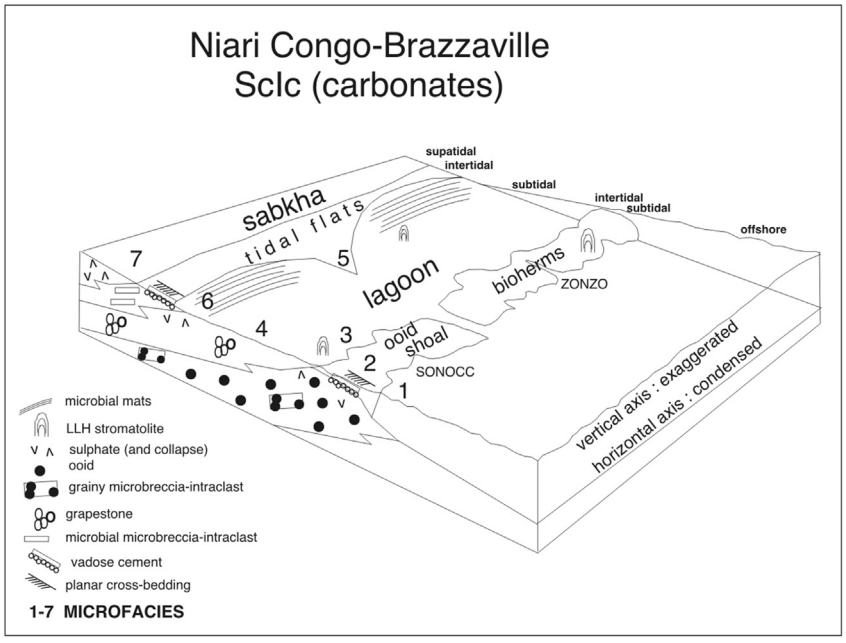

Fig. 9. Model for proximal shelf with an ooid ramp-edge shoal complex (SONOCC area) or reefal cone-shaped stromatolitic bioherms (ZONZO area) in the SCI_c series (systematic sampling of the series is metric to inframetric). Ramp-edge sedimentray bodies are kilometer long and developed during weak sea level rise. Microfacies 1 to 7 succession represents the standard sequence for the series.

microstalactitic cementation (Fig. 6H). The larger ones, representing sub-spherical vadoids (pisoids), are mixed in the sediment without a preferential orientation. Most of the ooids suffered to some extent replacement by rosettes of former sulphate with anhydrite relics, their internal surface is corroded and pyritized, they also suffered dissolution and replacement by dolospar. The nucleus of the ooids is often composed of a former sulphate mineral with anhydrite relics. Euhedral, authigenic bipyramidal quartz crystals are present in the nucleus and the periphery of ooid margins. Shelter-cavities ('umbrella-type'), up to a few mm long, are common below elongated intraclasts. They contain internal sediment and are occluded by whitish bladed and granular Fe-calcite cements (staining coloration). This microfacies, typically with medium-to thick-bedded sedimentary structures on the field,

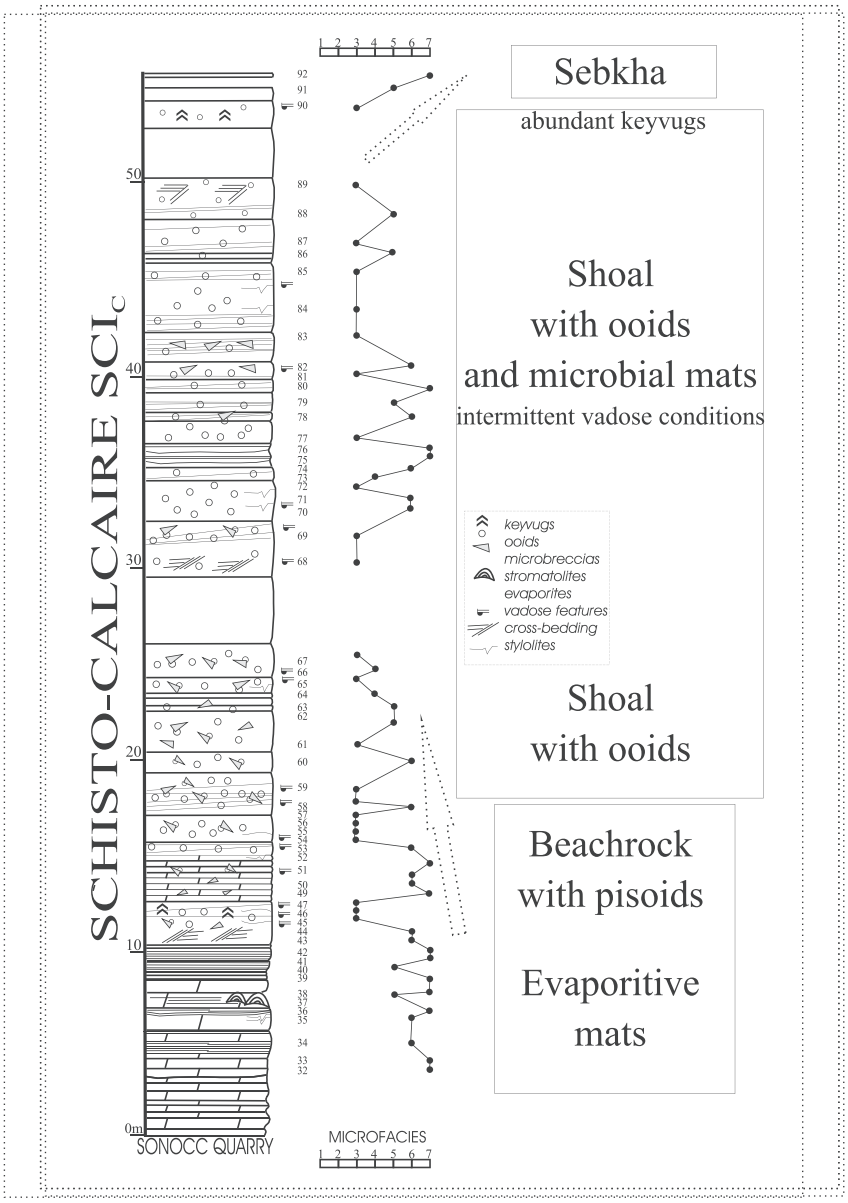

Fig. 10. Stratigraphic section of the SONOCC (MAD8150) quarry exposing the SCI_c Formation, sample location, lithologic curve (from standard MF1-MF7 microfacies succession), sedimentological interpretations. Microfacies 1 to 7 succession represents the standard sequence for the series. Explanation in text. Dashed arrows represent slow relative sea level rise (lower arrow) and more prononced relative sea level fall (upper arrow). High frequency fifth-order cycles defined by repetitive sea level fluctuations mainly from MF2 to MF6 are the fundamental building blocks of the series.

includes a dominant planar stratification and asymmetrical current ripples, cross-bedding sometimes with bidirectional foresets. It overlies the bioherms and sometimes interfinger with these reefal facies.

Environment: The various forms of internal cross-stratification indicate the action of multiple depositional processes in a shallow water environment where ooids formed. This microfacies represents sand belts or sandy shoals submitted to vadose conditions as indicated by the pendulant cements and internal sediments. This microfacies was probably affected by evaporite reflux or hypersaline conditions as shown by the crystal growth of sulphate in the ooids. Examples of modern ooids displaying radial fabric occur in hypersaline brines within Great Salt Lake, Utah (Reitner et al., 1997). Former hypersalinity is also suggested by euhedral authigenic quartz (Shukla and Friedman, 1981; Mamet and Préat, 2005). Planar stratification is the result of upper-flow regime storm current that destroyed the normal tidal bedforms (Clough and Goldhammer, 2000) and produced the intraclasts mixing all the grains together, including eroded grapestones from nearby tidal environments (discussed below, MF4) including those having submitted to vadose conditions.

4.3.2.3. Microfacies 3 (MF3): intertidal sandy ooid shoal (beachrock). This microfacies is similar to the previous one, and the main difference consists of the presence of mixed proto-oolites, bimodal size-distribution of the ooids, abundant sulphate microcrystals (30 μm, very similar to polyhalite determined by X-ray diffractometry in coeval series if the Lower Congo region, Delpomdor, 2007). These grains form sometimes thin levels in the mud-supported facies, and meniscus cementation between the grains suggets a beachrock sediment with millimeter-sized keystone vugs in the ooid dolograinstone (Fig. 7A). Cementation is similar to that

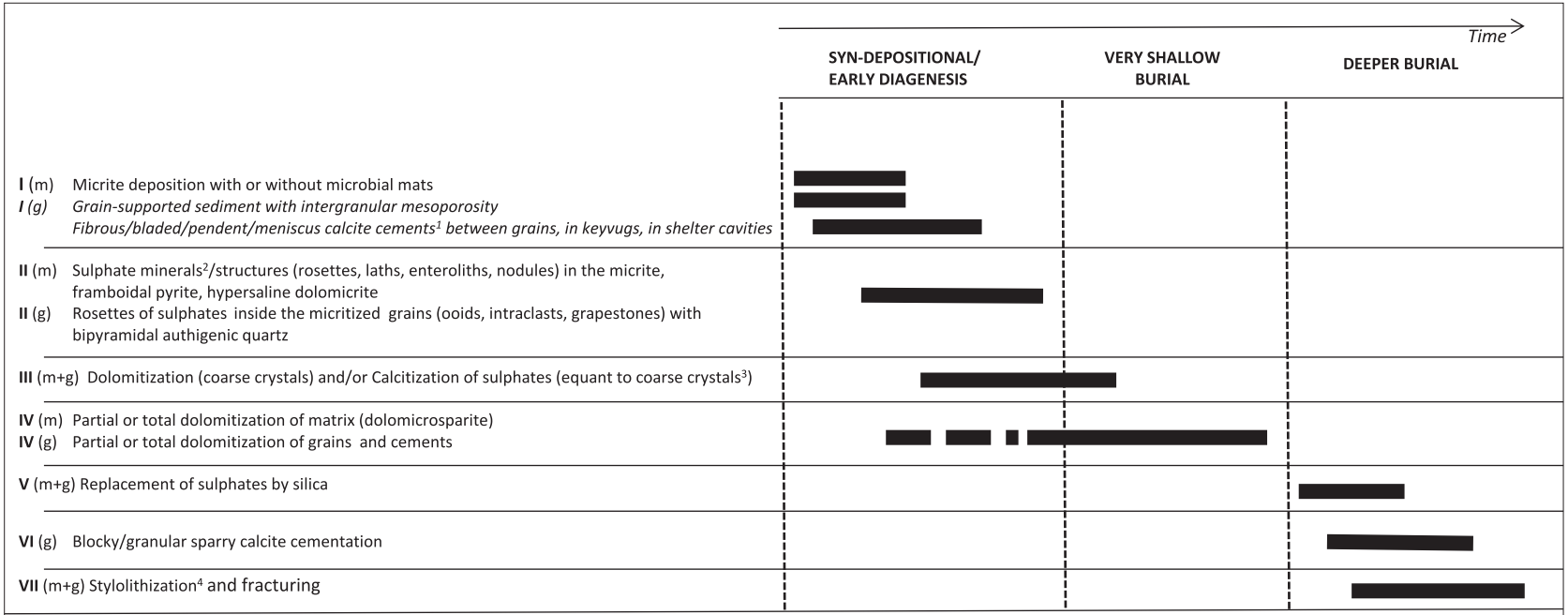

Paragenetic sequence of the SCIc carbonates (Comba Basin). In the diagram (m) is for mud-supported fabrics, *(g) is for grain-supported fabrics*.
The sequence is driven by alternative evaporitive and meteoric phases as highlighted by petrography and stable isotopes (see text).
[1] most of the cements are isopachous
[2] sulphate minerals are mainly anhydrite, nodules are up to one centimeter-sized. Soft synsedimentary deformations are common (microteepes)
[3] sometimes with two cement generations, with a dissolution stage
[4] very pronounced in the grain-supported facies (up to 10 cm of amplitude)

Fig. 11. Paragenetic sequence of the SCIc carbonates (Comba Basin).

of MF2b with common microstalactitic calcite cements associated with the ooids. These cements are randomly distributed suggesting that the grains have been reworked from their depositional environment (vadose), or they display curved surfaces reflecting meniscus surfaces of the water concentrated at the grains contacts at the time of precipitation. The various forms of internal cross-stratification are similar to the previous facies with important cross-bedding (Fig. 7B). The facies is sometimes interstratified with dolowackestones containing proto-oolites. Stylolites are often well developed and are characteristic of the massive beds (>1 m) observed in the field, which are almost composed of well-sorted oolites (Fig. 2C). It should be noted here that the stylolites are recurrent throughout the SCIc series and are observed in all facies (and microfacies). They are best developed in the grainy oolitic facies and have spectacular amplitudes up to 10 cm. They thus constitute a criterion for identification on the field or in boreholes of the oolitic facies richest in calcium carbonate, which are very sought after by the cement industry. Fracturing is regularly present in all the facies but not excessive. The fractures, opening up in various directions, are filled with calcite and intersect either the matrix in the mud-supported fabrics or the grains (ooids, intraclasrs …) and cements in the grain-supported fabrics. The are discontinuous (mm-cm length) and for the most less that 1 mm wide.

Environment: As the previous microfacies (MF2), this microfacies consists of high-energy environments, the beachrock and vadose cements within the grainstones indicate local subaerial exposure on 'islands' or on top of the shoals. The presence of bimodally sorted oolites, proto-oolites, and interstratification with dolowackestones reveal the proximity of a back-shoal environment or an inner shoal. Large ovoid to rounded keystone vugs are also observed in the pure oolite facies. The importance of cross-bedding suggests that the facies may represent an active crest of a sand shoal where ooids formed (Harris and Fraunfelter, 1993). Tops of shoal deposits experiencing higher current energies and depositing cleaner grainstones-rudstones have concentrated active diagenetic fluids and brines. It resulted intense cementation, dolospar replacement and precipitation (of dolomite and calcite) in the grain-supported facies, input (eolian polyhalite?) and precipitation of sulphate minerals (with anhydrite relics) in the mud-supported fabrics. By comparison to modern oolitic sands, water depth was no more than a few meters (Wagner and van der Togt, 1973). Numerous samples containing almost nothing than ooids (>90%) were probably deposited in water less than 2 m, the optimum zone of ooid production (Purser and Evans, 1973). The keystone vugs form immediately above the wave swash zone in the beach environment (Esteban and Klappa, 1983). They are produced in the uppermost laminations of the beach accretion beds (Dunham, 1970) as a result of air escaping from intergranular pores as they are floored with marine waters during the flood tidal cycle (Inden and Moore, 1983). Microfacies 3 represents a shoal complex that was overprinted with subaerial and marine-hypersaline during early vadose diagenesis.

4.3.3. Tidal flats

4.3.3.1. Microfacies 4 (MF4): tide-dominated lagoonal environments. This microfacies consists of greyish to blackish fine-grained peloidal laminar and non laminar dolomudstones, dolowackestones and dolopackstones with small-sized micritized ooids (50–150 μm), subcentimetric grapestones, silty quartz and feldspar grains, tiny sulphate minerals (polyhalite?) and fine-graind pyrite. Larger non-micritized oolites (0.5 mm) are also observed as some intraclasts from reworked microbial mats (bindstone). Wavy stromatolites are commonly observed with sub-millimeter-scale undulatory and planar laminae alternating with dark grey laminae. The dolomicrite matrix contains replaced leached laths and acicular rods of sulphate (with anhydrite relics, gypsum) forming the nucleus of the oolites.

Environment: These predominantly mud-supported facies were deposited in semi-protected areas behind ooids shoals. Larger ooids were probably swept off of nearby shoals during large storms and deposited in these leeward areas. Grain types are predominantly small-sized ooids, grapestones and former sulphates.

4.3.3.2. Microfacies 5 (MF5): nearshore channeled belt. Thin-to medium bedded, millimetre-thick slightly laminar intraclastic peloidal dolopackstone/dolograinstone and homogeneous dolomudstone with small-sized sulphate minerals, fans of silt-sized sulphate crystals and abundant small-sized spheroidal pyrite. The laminae are not well defined, they are cross-stratified with low to medium angle, planar or undulatory to tufted-crinkly. Associated sedimentary structures include desiccation mud-cracks, poorly defined laminoid fenestral fabric and small-sized shelter cavities. Intraclasts are elongated (up to 6 mm long, 0.5–3 mm thick), sometimes subrounded, well sorted, and consist of microbial mats with desiccation cracks. They contain euhedral authigenic bipyramidal quartz crystals.

Environment: Parallel laminite represents fairly rapid mechanical deposition by weak currents and settling of mud from suspension in an upper intertidal to supratidal setting (Clough and Goldhammer, 2000). This facies formed in tidal channels systems, which were floored with microbial intraclasts coming from the levees. As suggested by the desiccation cracks, these channels were very shallow, may be a few decimeters deep as reported in the intertidal channels of Andros Island, Bahamas (Hardie and Garett, 1977) and, were episodically submitted to vadose conditions (shelter cavities). As for the previous facies, microfacies 5 suffered hypersaline conditions as shown by the pseudomorphs of evaporitic minerals.

4.3.3.3. Microfacies 6 (MF6): inland microbial marsh. Greyish thin-to medium bedded, finely laminated homogeneous dolomudstone and dolomicrosparite. The dolomudstone layers are undulating, infra-to plurimillimeter-thick, and constituted by remnants of probable cyanobacterial mats which suffered a diagenetic alteration leading to a typical 'peloidal-alveolar' texture with peloids and breccias. These latter consist of small-sized monomictic mudchips exhibiting a 'jigsaw puzzle'. Laminae are primarily produced by the alternation of organic-rich and organic-poor horizons. They consist of flat-laminated microbial mats or 'cryptomicrobialites' and domal stromatolitic columns (LLH *sensu* Logan et al., 1964) up to decimeter-height in the field. Parallel laminite consists of millimeter-scale planar, wavy and very low-angle cross-stratified laminae composed of well-sorted carbonate mud and small-sized sulphate minerals giving a whitish color to the laminae. The muddy and microsparitic matrices contain dispersed idiotopic dolomite rhombs (up to 50 μm). The laminae are sometimes slightly slumped and exhibit an irregular lenticular fabric with pseudomorphs of sulphate. They are also slightly deformed by crystallization of sulphate minerals inducing the formation of microtepees.

Environment: Micritic, millimeter-scale laminae interlayered with organic-rich thin levels (benthic microbial mats) associated with thin autobrecciated layers and numerous mudcracks point to a tidal flat environment (Purser, 1973; Hardie and Ginsburg, 1977; Sellwood, 1986; Clough and Goldhammer, 2000). Evaporitic conditions were also present as indicated by various microtepee structures or nodules (on the field) and dolomitic pseudomorphs after sulphate crystals with anhydrite relicts.

4.3.4. Evaporative environments, sabkha

4.3.4.1. Microfacies 7 (MF7): littoral lagoon and sabkha. Well (millimeter-centimeter) to poorly stratified darkish dolomudstone (Fig. 7A), and yellowish and whitish dolomicrosparite with remnants of microbial mats (Fig. 7B). Slumping and small-scale folding are regularly observed (Fig. 7E and F). The replacement could be extensive and the former sulphate minerals, which can represent 50% or more of the sediment (Fig. 7G), contain abundant dolomite relics. As microsparitization increases whitish color is more pronounced in hand specimen and thin section is quite transparent. Evaporite (anhydrite, gypsum and polyhalite?) minerals are common in the matrix and consist of lath-shaped (Fig. 7D), rosette-like aggregates (Fig. 7H), enterolithic small-sized nodules, veins, collapse breccias and castellated crystals (*sensu* Clark, 1980), which often grew inside the mats (intrasedimentary growth). Lath-shaped and rosette-like aggregates are sometimes partially or totally replaced by amoeboid silica forming juxtaposed zones of 50–150 μm.

Environment: The observed sedimentary structures point to a general peritidal environment analogous to present littoral lagoons or sabkhas formed under warm semi-arid conditions, such as can be seen along the Persian Gulf.

4.4. Diagenesis and sedimentary model

The Schisto-Calcaire Group consists predominantly of dolomitized grain-supported and mud-supported carbonates with abundant ooids, intraclasts, microbial and stromatolitic textures (silt- and sandchips, laminae, domes), pseudomorphs of evaporitic minerals and less abundant grapestones, peloids and fenestral fabrics. Dolomitization was probably early diagenetic through the interaction with near-coeval brines (microfacies 7). The micritic matrix is partly to totally replaced by a fine crystalline hypidiotopic to idiotopic dolomite. Hypersaline conditions developed and microenterolithes replaced progressively the muddy matrix with typical thin slumped and folded layers. Early dolomitization is evidenced by excellent fabric retention during dolomitization of highly soluble evaporitic phases as reported for example in the Mesoproterozoic of the Society Cliffs Formation in the Northern Baffin Island (Kah, 2000). Similarly, to the Schisto-Calcaire series of SW Gabon (particularly in the Nsc3 Formation, Préat et al., 2010), the depositional paleoenvironment of microfacies 4 to 7 of our studied series is interpreted as peritidal possibly representing small intertidal and supratidal ponds. In most of the grain-supported sediments of our study, the intergranular fibrous cements are replaced by equant and granular white calcite crystals. Most of the grains (mud- and grain-supported sediments) have been replaced by these calcite crystals. Isopachous equant and microstalactitic white calcite cements were associated with phreatic and vadose meteoric waters respectively, affecting most of the porous grain-supported sediments. Large fenestrae related to crinkled microbial mats indicate that the substrate was temporarily exposed to quiet water conditions. Evaporitic conditions were also present as indicated by various tepee structures or nodules (in the field) and dolomitic pseudomorphs after sulphate crystals with anhydrite relics.

The ooid packstones and grainstones in the SONOCC (SCI_c Member) quarry and the stromatolite bioherms of the ZONZO section represent a mid-ramp shoal-water carbonate complex or carbonate-bank assemblage with high-energy conditions (microfacies 2 and 3) surrounded by belts of lower energy facies, with a seaward outer ramp shallow-water open shelf (microfacies 1) and a landward backshoal restricted inner ramp (microfacies 4 to 7) with episodically hypersaline conditions (microfacies 7). Comparison to well known modern areas of carbonate deposition, such as the Bahamas and the Persian Gulf, indicates water depths of 0–30 m over most of the Schisto-Calcaire Group.

The ooid shoals are coeval with the C3 Formation of the DRC (Cailteux et al., 2015; Delpomdor et al., 2015) suggesting that these shoals were extensive and formed broad sand belts. Although the geometry of deposits of the SCI_c Formation is seen as continuous on the southern edge of the Chaillu Massif, Chorowitz et al. (1990) concluded that the Lower Congo/Sangha aulacogen, extended to the Comba Basin, shows multiple pull-apart-type tectonic areas constituted of elongated WNW-ESE tilted blocks limited by NE-SW faults. Therefore, the deposits appear to be diachronous favouring the development of oolitic barriers on the high positions. However, in the absence of conclusive field observations, the development of a cordon of oolitic sands of the C3 Formation in the DRC (see Fig. 3), similar to the SCI_c Member of the Republic of Congo, may be deposited on the NW edge of the Kasaï block (Figs. 1 and 12).

5. Geochemistry

5.1. Data presentation (Fig. 13 and Table 2)

The SCI_a dolomudstones have stable isotope compositions ($\delta^{18}O$ and $\delta^{13}C$) consistent with those of the Cap Carbonates reported by Shields (2005) and Kennedy et al. (2008) in Australia. In our data (Kengué section: MAD0158; Mousa River section: MAD0198 and; Makoubi quarry: SB0015), the SCI_a isotopic compositions are grouped (Figs. 7 and 8) near a mean value of −6.4‰ ($\delta^{18}O$, n = 42) and −3.5‰ ($\delta^{13}C$, n = 42) and there is no correlation between $\delta^{18}O$ and $\delta^{13}C$ (r = −0.3, n = 42). These isotopic values are the same as those reported in SW Gabon ($\delta^{18}O$ = −6.3‰, n = 8 and $\delta^{13}C$ = −3.2‰, n = 8; Préat et al., 2011). The vertical pattern of carbon isotope values shows a general trend or shift to slightly more depleted from the base to the top of the Cap Carbonate series. This is particularly observed in the two profiles of Mousa River section (MAD0198: 10.5 m thick) and Makoubi quarry (SB0015: 12.6 m thick), with a 1.3‰ shift of the isotopic composition of the carbon, from −3.2‰ at the base of the series and −4.5‰ at the top. In Kengué section (MAD0158), the values do not present a significant shift. These shifts have been already reported in coeval series in the Lower Congo region (Delpomdor and Préat, 2013). As in SW Gabon, the Cap Carbonate $\delta^{13}C$ of the Schisto-Calcaire Group are slightly more negative than those reported for typical 'Marinoan' event, ranging form −1‰ to −5‰ (Hoffman and Schrag, 2002) and strongly negative if compared to the overlying SCII (and SCIII) carbonates with values ranging between −3‰ and +2‰ (Fig. 7). The SCI_a oxygen isotopic values are well grouped with no particular trend. They are in the range of those of the Neoproterozoic ocean (Jacobsen and Kaufman, 1999; Halverson et al., 2005). These $\delta^{18}O$ values (Fig. 13, Table 2) record oceanic precipitation during post-glacial sea level rise (Préat et al., 2011; Mickala et al., 2014).

The medium-bedded ooid, stromatolitic and evaporitic SCI_c dolostones show stable isotope features in a narrow domain (except for two samples, cb91 and cb92) and there is no stratigraphic trend at the scale of the series in the SONOCC (MAD8150) and ZONZO (MAD0165) sections. All $\delta^{18}O$ values (excepting those concerning evaporitic samples cb91 and cb92, discussed below) vary from −10.2‰ (sample cb31, SONOCC) to −9.0‰ (sample cb63, SONOCC), with an average of −9.3‰ (n = 45), similarly all $\delta^{13}C$ values (excepting those concerning samples cb91 and cb92) vary from −4.1‰ (sample cb136, ZONZO) to −2.8‰ (sample cb82, SONOCC) with an average of −3.8‰ (n = 45). There is no correlation between $\delta^{13}C$ and $\delta^{18}O$ in the SCI_c samples (r = −0.6). The SCI_c $\delta^{18}O$ values are lighter (>1.5‰ on average) than those of the Neoproterozoic ocean (Jacobsen and Kaufman, 1999; Halverson et al., 2005) and lighter (>3‰ on average) than those of our Cap

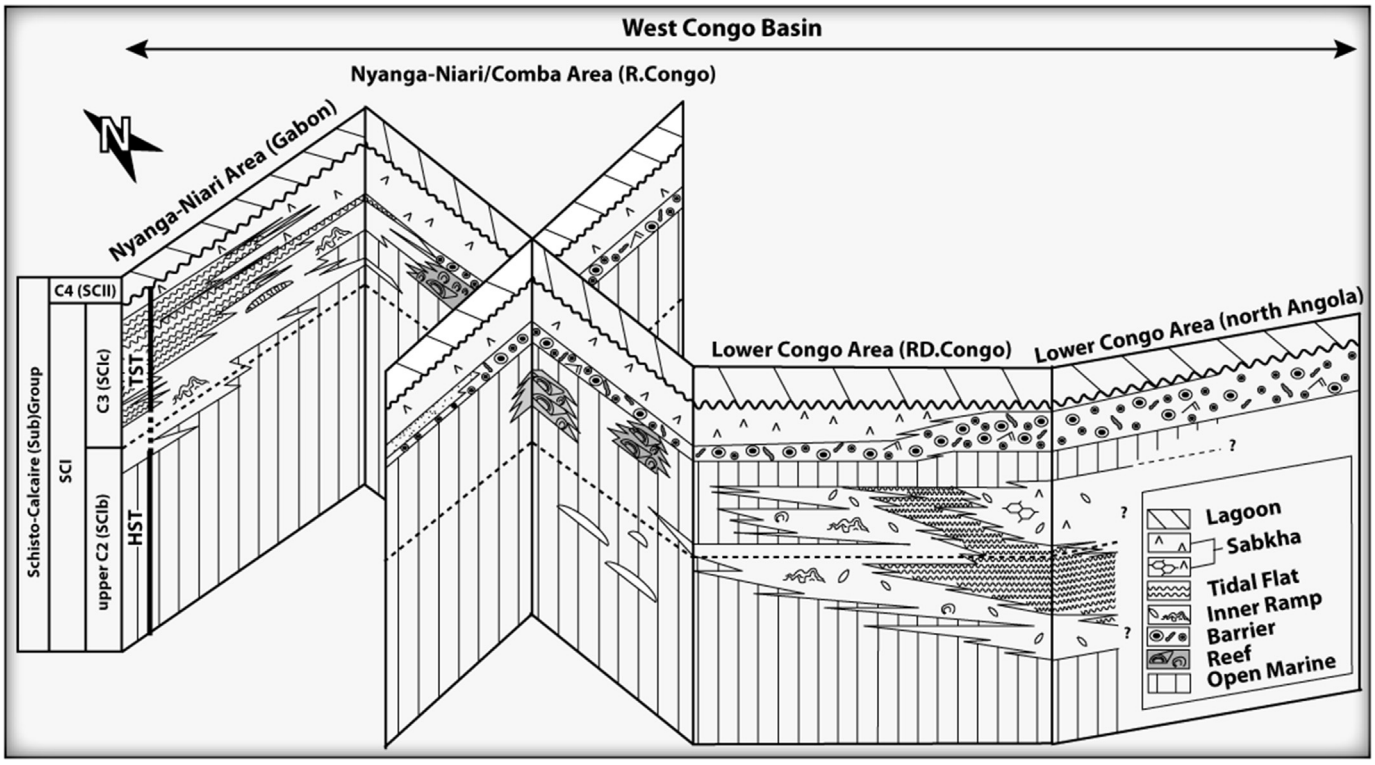

Fig. 12. Cartoon with reconstructed stratal geometry for the SCI_c unit (lower part of the Schisto-Calcaire Group) coupled with depositional models in the Neoproterozoic West Congo Basin with distinct areas (Nyanga-Niari, Comba, Lower Congo, northern Angola) projected onto a longitudinal line of NW-SE orientation (after Delpomdor et al., 2015).

Carbonate (SCI_a) samples. The average $\delta^{13}C$ values of the SCI_c and SCI_a are the same. Samples cb91 and cb92, collected at the top of the SONOCC quarry (MAD8150), consist of homogeneous evaporitic dolomudstones with very abundant needles and laths of sulphate (anhydrite) typical of a sabkha deposition (our MF7). Compared to the $\delta^{18}O$ values of all other SCI_c samples these two samples have $\delta^{18}O$ strongly heavier by 5‰ values (−5.4‰, cb91). Sample cb92 (top of the section) has a very negative $\delta^{13}C$ value also different and lighter (by more than 4‰) than those of the SCI_c samples (Fig. 13). Two oolite samples with keystone vugs (MAD0202) encompassing the SCI_b/SCI_c succession yield the same carbon and isotopic values to those of the $SC1_c$ previously reported. However their accurate stratigraphic location is uncertain.

The $\delta^{18}O$ and $\delta^{13}C$ from the SCII (and SCIII) successions range respectively from −9.6‰ (MAD0183) to −4.1‰ (MAD8149), and from −3.7‰ (MAD0213) to +8.4‰ (MAD0177) with $\delta^{18}O$ average value of −6.7‰ and −1.0‰ for the $\delta^{13}C$ (n = 41). Despite the accurate stratigraphic location of these samples is not sure due to discontinuous outcrops, the result shows that there is a very weak correlation (r = +0.4) between $\delta^{13}C$ and $\delta^{18}O$ in the SCII (and SCIII) successions with a general increase of values from SCII to SCIII formations.

Of particular interest are the samples collected in the Bouenza and the Upper Tillite formations, overlain by the Schisto-Calcaire Group (Fig. 2). This series does not crop well in the area, particularly the Bouenza Formation: five samples have been collected, one in the oolitic dolograinstone in the Bouenza Formation (MAD0226) and 4 cm-sized clasts of oolitic dolograinstones in the matrix of the overlying Upper Tillite (MAD0196 and MAD0225). These clasts probably represent rock fragments of the Bouenza Formation. The $\delta^{18}O$ values of MAD0226 sample and one MAD0225 sample are slightly outside of the marine domain, while the second MAD0225 sample displays a marine signature (Fig. 13). In contrast, the $\delta^{13}C$ values of the three samples are strongly enriched in ^{13}C (values around +11.1‰, Fig. 13). In MAD0196, the samples have highly negative $\delta^{18}O$ values (−11.8‰) and $\delta^{13}C$ values near 0‰.

5.2. Interpretation

A crucial question in any study of carbonate chemostratigraphy is whether a primary marine signature is preserved (Fairchild et al., 2000). Jacobsen and Kaufman (1999) modelled the $\delta^{18}O$ and $\delta^{13}C$ isotopic evolutions of Neoproterozoic seawater, their values are reported in Fig. 13. These values have been confirmed by Halverson et al. (2005) and the best estimate of the average original carbonate $\delta^{18}O$ composition is −7‰ to −7.5‰ at ~0.5–0.6 Ga (from Fig. 1 *in* Kasting et al., 2006). The $\delta^{18}O$ values of the SCI_a (average −6.4‰, n = 42), SCII (except two samples in MAD0183) and SCIII carbonates are therefore in the range of the marine values. The SCI_a average $\delta^{18}O$ values can be considered as representative of the pristine marine signal as this series formed on the transgressive surface during post-glacial sea level rise on the Upper Tillite. The heavy oxygen isotopic values (up to −4.0‰, MAD8149, up to −4.8‰, MAD0220; Fig. 13) are probably primary or early diagenetic related to an evaporative enrichment of shallow-marine waters which led to an elevated $\delta^{18}O$ composition (Land, 1980; Tucker and Wright, 1990; Préat et al., 2010). These heavier values are consistent with petrographic evidence of evaporitic dolomudstones and fine-to medium-grained dolomicrosparites partly or totally replacing coeval sulphates (nodules, laths, rosettes, see microfacies 6 and 7).

Detailed sampling in the SCI_c Member does not reveal differences in oxygen- and carbon-isotope compositions within mud- and grain-supported fabrics, the isotope values are homogeneous or well grouped and have values that vary over a very narrow range of less than 2‰ (Figs. 13 and 14). There are also no differences in the oxygen- and carbon-isotope compositions between the

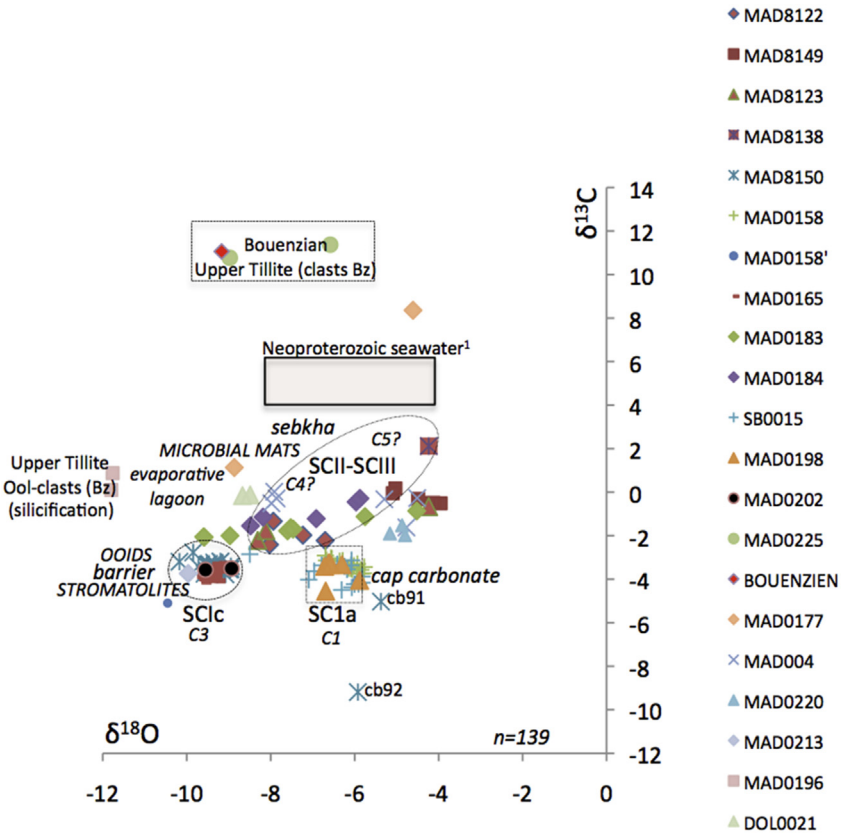

Fig. 13. Cross-plot of $\delta^{13}C$ versus $\delta^{18}O$ for carbonate rocks of the Schisto-Calcaire Group of the Comba Basin from 139 selected samples (values in Table 2). Formations SCI to SCIII, *sensu* Dadet (1969) (Fig. 3), Formations 'C1 to C5' refer to the coeval formations in the Lower Congo region (Fig. 3) *sensu* Delpomdor and Préat (2015). All values are reported in per mil relative to V-PDB by assigning a $\delta^{13}C$ value of +1.95‰ and a $\delta^{18}O$ value of +2.20‰ to NBS19. Reproducibility was checked by replicate analysis of laboratory standards and is better than ±0.04‰ (carbon) and 0.07‰ (oxygen) (1 sigma). [1]Isotopic composition of Neoproterozoic seawater is derived from Jacobsen and Kaufman (1999). Geographic and stratigraphic positions are given in Table 1 (Bz is for Bouenza Formation). See text for explanations.

dolomicrites and the dolomicroparites (compare for example isotopic values of cb120/136/137 with those of samples cb1331/132/133/135, Table 2). The $\delta^{18}O$ record in the SCI_c Member (average of −9.3‰, n = 45), suggests that meteoric waters flushed the series after the deposition of the 12 m thick Cap Carbonate succession (average $\delta^{18}O$ of −6.4‰, n = 42) and the $SC1_b$ siltites. The 50–90 m thick SCI_c shallow-water carbonates being younger than the SCI_a and SCI_b series (Figs. 2 and 3), a temperature effect due to burial can be dismissed (see below). This is also supported by petrography with fine-grained microspar replacing the mud-supported fabrics and equant and granular Fe-calcite replacing former sulphates and or precipitating in the remaining pores in the grain-supported fabrics.

The large variation in $\delta^{13}C$ isotope values points to different original marine waters as all the values are different of those reported for seawater (Fig. 13, Jacobsen and Kaufman, 1999). The distribution of the $\delta^{13}C$ values appears to be related to stratigraphy, with the same values in the SCI_a ($\delta^{13}C$, −3.4‰, n = 46), except samples cb91/cb92, and SCI_c (−3.8‰, n = 45) members. The carbon isotopic composition (n = 41) of the SCII and SCIII (only one sample was analysed in the latter, Table 2) formations do not fit a particular domain and vary from −2.0‰ (MAD0183) to +2.1‰ (MAD8138) with one outlier (+8.4‰, MAD0177). The $\delta^{13}C$ value of a carbonate collected in the Bouenza Formation (MAD0226) shows a very high value as those of the oolitic clasts in the overlying Upper Tillite. However, two Bouenzian oolite clasts in the Upper Tillite (MAD0196) do not show significant deviation from the average $\delta^{13}C$ of the Schisto-Calcaire Group. The Bouenza Formation (only one studied sample) and carbonate clasts in the Upper Tillite (four samples) need more studies. These clasts are rare in the Upper Tillite and the Bouenza units does not crop well and is predominantly clastic.

6. Discussion and conclusions

Considering only the SCI_c succession, the $\delta^{18}O$ record shed light on the recycling of the freshwater surface. The $\delta^{18}O$ values (n = 45) are well grouped (Fig. 13), range from −10.2 and −9.0‰ (except samples cb91 and cb92, discussed below) and are less negative than those of the underlying SCI_a. Since the SCI_c succession is younger than the SCI_a series (Figs. 2 and 14), a temperature effect due to burial can be dismissed and a freshwater influx has to be considered. $\delta^{18}O$ and $\delta^{13}C$ co-variation at a larger scale (Fig. 12) can support this interpretation because such negative $\delta^{18}O$ suggest a greater introduction of photosynthetically depleted ^{13}C from subaerial recharge area (Knauth and Kennedy, 2009). A similar negative carbon isotope excursion is present in the same area in the lower part ('Nsc1') of the Schisto-Calcaire of SW Gabon by Préat et al. (2011). This means that this meteoric water flushing was regional and not local and could record a climate evolution from an arid period with the hypersaline conditions (e.g., microfacies 7) to more humid conditions (e.g., the meteoric cements in the grain-supported fabrics). Although the timing of the series is poorly constrained in order to establish detailed correlations between the lower part of the Schisto-Calcaire Group in SW Gabon (Préat et al., 2010), Lower Congo region (Delpomdor and Préat, 2013, 2015;

Table 2
Isotopic values ($\delta^{13}C$, ‰VPDB and $\delta^{18}O$, ‰VPDB) of selected samples from the Schisto-Calcaire Group of the Comba Basin. cb: Congo-Brazzaville, MADxxxx, DOLxxxx: Madingou and Dolisie areas, number 'xxxx' refers to GPS location, cc: Cap Carbonates, SCI_a, SCI_c, $SCII_{b/c}$, $SCII_c$, SCIII: succession of the members of the different formations (see Fig. 3), SONOCC: active Loutété quarry and ZONZO: cliff in a hill in the Zonzo area (see Table 1 and Fig. 1), Riv: River, evap: Evaporite, HCS: Hummocky Cross Stratification.

Oxygen and carbon isotopic data, location of sections, stratigraphy, microfacies, Bouenzian, Upper Tillite and Schisto-Calcaire series (Comba Basin). Explanations in text.

Sample	$\delta^{18}O$ ‰[a] (‰VPDB)	$\delta^{13}C$[a] (‰VPDB)	Location	Stratigraphy	Description	Remarks
cb3	−6,70	−2,22	MAD8122	SCII	doloconglomerate (L)	ooids, intraclasts (mats)
cb6	−7,23	−1,98	MAD8122	SCII	dolomicrite-dolomicrosparite	
cb7	−8,03	−2,41	MAD8122	SCII	dolomicrosparite	sulphates, microbial mats
cb9	−7,94	−1,34	MAD8122	SCII	dolomicrite-dolomicrosparite (L)	stromatolite
cb12	−5,03	0,17	MAD8149	SCII	dolomicrite-dolomicrosparite	sulphates
cb14	−4,12	−0,49	MAD8149	SCII	dolomicrite-dolomicrosparite	
cb17	−4,15	−0,49	MAD8149	SCII	dolomicrite-dolomicrosparite (L)	sulphates
cb18	−3,95	−0,51	MAD8149	SCII	dolomicrosparite	hardgrounds
cb19	−4,49	−0,31	MAD8149	SCII	dolomicrite-dolomicrosparite	sulphates, pyrite
cb25	−5,09	−0,05	MAD8149	SCII	dolomicrite	sulphates
cb27	−4,24	−0,67	MAD8123	upper? SCII	dolomicrite-dolomicrosparite	microslumps
cb30	−8,31	−2,22	MAD8123	upper? SCII	dolomicrosparite	collapse, veins
cb31	−8,12	−1,76	MAD8123	upper? SCII	dolomicrosparite	sulphates
cb32	−4,23	2,12	MAD8138	SCIIc	dolomicrite-dolomicrosparite	sulphates
cb34	−10,17	−3,20	MAD8150	SCIc	dolomicrite-dolomicrosparite (L)	intraclasts (mats)
cb38	−8,99	−3,55	MAD8150	SCIc	dolomicrosparite (L)	mats, silt
cb39	−9,51	−3,60	MAD8150	SCIc	dolomicrite	sulphates
cb41	−9,32	−3,29	MAD8150	SCIc	dolomicrite-dolomicrosparite (L)	sulphates, microslumps
cb45	−9,48	−3,42	MAD8150	SCIc	dolofloatstone (S)	ooids, pendulant cement
cb47	−9,51	−3,32	MAD8150	SCIc	dolograinstone (S)	pisoids, sulphates
cb49	−9,58	−3,74	MAD8150	SCIc	dolomicrite (L)	sulphates
cb52	−9,42	−3,67	MAD8150	SCIc	dolomicrite	sulphates
cb54	−9,33	−3,35	MAD8150	SCIc	dolograinstone (S)	pisoids, pendulant cement
cb58	−9,35	−3,23	MAD8150	SCIc	dolograinstone (S)	pisoids, pendulant cement
cb63	−8,96	−3,54	MAD8150	SCIc	dolopackstone (S)	pisoids
cb65	−9,47	−3,30	MAD8150	SCIc	dolopackstone (S)	pisoids, sulphates
cb66	−8,95	−3,40	MAD8150	SCIc	dolomicrite	
cb69	−9,20	−3,19	MAD8150	SCIc	doloconglomerate (S)	pisoids, sulphates
cb72	−9,20	−3,20	MAD8150	SCIc	doloconglomerate (S)	pisoids, sulphates
cb76	−9,72	−3,42	MAD8150	SCIc	dolomicrite	
cb79	−9,08	−3,78	MAD8150	SCIc	dolowackestone (L)	sulphates
cb82	−9,85	−2,77	MAD8150	SCIc	doloconglomerate (S)	pisoids, sulphates
cb89	−9,30	−3,54	MAD8150	SCIc	dolograinstone	ooids
cb91	−5,37	−5,03	MAD8150	SCIc	dolomicrite (chalky)	very abundant sulfates
cb92	−5,92	−9,19	MAD8150	SCIc	dolomicrite (L)	very abundant sulfates
cb94	−6,06	−3,54	MAD0158	SCIa	dolomicrite-peloidal packstone (L)	loferitic fabric
cb95	−5,94	−3,54	MAD0158	SCIa	dolomicrite-peloidal packstone (L)	loferitic fabric
cb96	−5.85	−3.57	MAD0158	SCIa	dolomicrite-peloidal packstone (L)	loferitic fabric
cb97	−6.10	−3.50	MAD0158	SCIa	dolomicrite-peloidal packstone (L)	loferitic fabric
cb98	−6.15	−3.49	MAD0158	SCIa	dolomicrite-peloidal packstone (L)	loferitic fabric, crust
cb99	−6.67	−3.14	MAD0158	SCIa	dolomicrite-peloidal packstone (L)	loferitic fabric, crust
cb100	−6.70	−2.91	MAD0158	SCIa	dolomicrite-peloidal packstone (L)	loferitic fabric, crust
cb101	−6.06	−3.50	MAD0158	SCIa	dolomicrite-peloidal packstone (L)	loferitic fabric, crust
cb102	−6.56	−3.04	MAD0158	SCIa	dolomicrite-peloidal packstone (L)	loferitic fabric, crust
cb103	−5.93	−3.30	MAD0158	SCIa	dolomicrite-peloidal packstone (L)	loferitic fabric, crust
cb104	−6.02	−3.39	MAD0158	SCIa	dolomicrite-peloidal packstone (L)	loferitic fabric
cb106	−6.54	−3.06	MAD0158	SCIa	dolomicrite-peloidal packstone (L)	loferitic fabric
cb107	−5.77	−3.45	MAD0158	SCIa	dolomicrite-peloidal packstone (L)	loferitic fabric
cb108	−6.28	−3.15	MAD0158	SCIa	dolomicrite-peloidal packstone (L)	
cb109	−6.36	−3.18	MAD0158	SCIa	dolomicrite-peloidal packstone (L)	
cb110	−5.79	−3.73	MAD0158	SCIa	dolomicrite-peloidal packstone (L)	
cb111	−5.95	−3.62	MAD0158	SCIa	dolomicrite-peloidal packstone (L)	
cb112	−5.84	−3.75	MAD0158	SCIa	dolomicrite-dolomicrosparite (L)	
cb114	−5.94	−4.06	MAD0158′	SCIb	dolosiltite	HCS
cb115	−10.45	−5.10	MAD0158′	SCIb	clayey dolosiltite	HCS
cb116	−9.47	−4.03	MAD0165	SCIc	doloconglomerate (S)	intraclasts (mats)
cb118	−9.65	−3.97	MAD0165	SCIc	collapse breccia	sulphates
cb119	−9.63	−4.12	MAD0165	SCIc	doloconglomerate	intraclasts (mats)
cb120	−9.41	−4.06	MAD0165	SCIc	dolomicrite (L)	intraclasts (mud)
cb121	−9.48	−3.92	MAD0165	SCIc	dolomicrite-dolomicrosparite	mats (relicts)
cb123	−9.49	−3.85	MAD0165	SCIc	dolomicrite-dolomicrosparite	collapse, veins
cb125	−9.51	−3.88	MAD0165	SCIc	collapse breccia	sulphates
cb127	−9.37	−3.82	MAD0165	SCIc	dolobindstone-dolomicrosparite (L)	stromatolite
cb128	−9.40	−4.00	MAD0165	SCIc	dolobindstone-dolomicrosparite (L)	stromatolite
cb129	−9.68	−3.99	MAD0165	SCIc	dolomicrite-dolomicrosparite	

(*continued on next page*)

Table 2 (*continued*)

Oxygen and carbon isotopic data, location of sections, stratigraphy, microfacies, Bouenzian, Upper Tillite and Schisto-Calcaire series (Comba Basin). Explanations in text.

Sample	$\delta^{18}O$ ‰[a] (‰VPDB)	$\delta^{13}C$[a] (‰VPDB)	Location	Stratigraphy	Description	Remarks
cb131	−9.52	−3.84	MAD0165	SCIc	dolomicrosparite	microbial mats
cb132	−9.38	−3.89	MAD0165	SCIc	dolomicrosparite (L)	microbial mats
cb133	−9.34	−4.07	MAD0165	SCIc	dolomicrosparite	sulphates
cb135	−9.73	−3.88	MAD0165	SCIc	dolomicrosparite	sulphates
cb136	−9.30	−4.07	MAD0165	SCIc	dolomicrite (L)	stromatolite
cb137	−9.26	−3.63	MAD0165	SCIc	dolomicrite (L)	stromatolite
cb139	−9.39	−3.65	MAD0165	SCIc	collapse breccia	sulphates
cb140	−9.38	−3.45	MAD0165	SCIc	dolobindstone-dolomicrosparite (L)	stromatolite
cb142	−9.26	−3.54	MAD0165	SCIc	dolobindstone-dolomicrosparite (L)	
cb143	−9.35	−3.42	MAD0165	SCIc	dolobindstone-dolomicrosparite (L)	stromatolite
cb144	−9.50	−3.46	MAD0165	SCIc	dolobindstone-dolomicrosparite (L)	
cb147	−9,37	−3,31	MAD0165	SCIc	dolobindstone	loferitic fabric
cb149	−9,21	−3,28	MAD0165	SCIc	dolobindstone-dolomicrosparite (L)	sulphates
cb155	−4,61	8,36	MAD0177	SCIII?	dolopackstone	ooids, sulphates
cb160	−8,87	1,13	MAD0180		dolomicrite	sulphates
cb163	−7,60	−1,78	MAD0183	SCIIb	silty dolomicrite	
cb164	−7,47	−1,70	MAD0183	SCIIb	silty dolomicrite (L)	sulphates
cb165	−7,52	−1,64	MAD0183	SCIIb	silty dolomicrite (L)	sulphates
cb166	−8,97	−2,00	MAD0183	SCIIb	silty dolomicrite (L)	sulphates
cb167	−5,75	−1,12	MAD0183	SCIIb	silty dolomicrite	sulphates
cb168	−4,52	−0,86	MAD0183	SCIIb	dolomicrite	
cb169	−9,58	−2,07	MAD0183	SCIIb	dolomicrosparite	sulphates
cb170	−9,60	−2,05	MAD0183	SCIIb	dolomicrosparite	sulphates
cb171	−8,48	−1,55	MAD0184	SCIIb	dolomicrosparite	sulphates
cb172	−8,18	−1,15	MAD0184	SCIIb	dolomicrosparite	sulphates
cb174	−5,97	−0,45	MAD0184	SCIIb	dolomicrite	sulphate rods-rosettes
cb174′	−5,88	−0,29	MAD0184	SCIIb	dolomicrite	sulphate rods-rosettes
cb177	−6,92	−1,22	MAD0189	SCIIb	dolomicrite-dolomicrosparite	sulphate rods-rosettes
cb179	−5,29	−0,33	MAD004	SCIIb	dolomicrite-dolomicrosparite	sulphate rods-rosettes
cb192	−7,92	0,02	MAD004	SCIIb	dolomicrosparite	mats (relicts)
cb193	−7,98	−0,51	MAD004	SCIIb	collapse breccia	sulphates
cb194	−4,77	−1,62	MAD004	SCIIb	dolomicrosparite	sulphates
cb196	−7,86	−0,29	MAD004	SCIIb	dolomicrosparite (L)	
cb200	−4,51	−0,27	MAD004	SCIIb	dolomicrite	sulphates
cb202	−10,01	−5,00	MAD0192	SCIb	dolomicrite (L)	
cb203	−9,93	−5,00	MAD0192	SCIb	dolomicrite (L)	
cb205	−11,77	0,87	MAD0196	Upper Tillite	clayey matrix	clast (oolite)
cb206	−11,80	0,10	MAD0196	Upper Tillite	clayey matrix	clast (oolite)
cb207	−6,56	−3,34	MAD0198	SCIa	dolomicrite-peloidal packstone (L)	loferitic fabric
cb207′	−6,72	−3,41	MAD0198	SCIa	dolomicrite-peloidal packstone (L)	loferitic fabric
cb208	−6,30	−3,33	MAD0198	SCIa	dolomicrite-peloidal packstone (L)	loferitic fabric
cb209	−6,60	−3,26	MAD0198	SCIa	dolomicrite-peloidal packstone (L)	
cb210	−6,62	−3,25	MAD0198	SCIa	dolomicrite-dolomicrosparite (L)	
cb212	−5,88	−4,05	MAD0198	SCIa	dolomicrite (L)	
cb213	−6,69	−4,55	MAD0200	SCIa	dolomicrite (L)	microslumps
cb214	−9,55	−3,57	MAD0202	SCIb/c?	dolograinstone	keystone vugs, ooids
cb215	−8,93	−3,51	MAD0202	SCIb/c?	dolograinstone	keystone vugs, ooids
cb216	−10,07	−3,32	MAD0206	SCIc	silty dolograinatone	bipyramidal quartz
cb217	−9,97	−3,74	MAD0213	SCIIb	dolomicrosparite	sulphates
cb220	−4,80	−1,98	MAD0220	SCIIb	dolomicrite	sulphate rods-rosettes
cb221	−5,16	−1,90	MAD0220	SCIIb	dolomicrosparite	sulphate rods-rosettes
cb222	−4,87	−1,53	MAD0220	SCIIb	dolomicrite	sulphate rods-rosettes
cb225	−8,98	10,77	MAD0225	Upper Tillite	clayey matrix	clast (oolite)
cb226	−6,58	11,37	MAD0225	Upper Tillite	clayey matrix	clast (oolite)
cb227	−9,17	11,06	MAD0226	Bouenzian	dolograinstone	ooids
cb229	−6,79	−3,36	SB0015	SCIa	brecciated dolomicrite	microfenestrae'?
cb230	−8,50	−2,85	SB0015	SCIa	dolomicrosparite	
cb231	−6,07	−3,13	SB0015	SCIa	dolomicrite	microfenestrae'
cb233	−6,41	−3,31	SB0015	SCIa	dolomicrite-peloidal packstone (L)	loferitic fabric
cb234	−6,18	−3,55	SB0015	SCIa	dolomicrite-peloidal packstone (L)	loferitic fabric
cb235	−6,55	−3,38	SB0015	SCIa	dolomicrite-peloidal packstone (L)	loferitic fabric
cb236	−6,09	−3,36	SB0015	SCIa	dolomicrite-peloidal packstone (L)	loferitic fabric
cb237	−6,24	−3,41	SB0015	SCIa	dolomicrite-peloidal packstone (L)	loferitic fabric
cb238	−6,68	−3,36	SB0015	SCIa	dolomicrite-peloidal packstone (L)	loferitic fabric
cb239	−6,97	−3,64	SB0015	SCIa	dolomicrite-peloidal packstone (L)	loferitic fabric
cb240	−7,10	−4,02	SB0015	SCIa	dolomicrite	
cb241	−5,82	−3,88	SB0015	SCIa	dolomicrite	
cb242	−5,91	−4,21	SB0015	SCIa	dolomicrite	

Table 2 (*continued*)

Oxygen and carbon isotopic data, location of sections, stratigraphy, microfacies, Bouenzian, Upper Tillite and Schisto-Calcaire series (Comba Basin). Explanations in text.

Sample	$\delta^{18}O$ ‰[a] (‰VPDB)	$\delta^{13}C$[a] (‰VPDB)	Location	Stratigraphy	Description	Remarks
cb243	−6,18	−4,23	SB0015	SCIa	dolomicrite (L)	
cb244	−5,82	−4,17	SB0015	SCIa	dolomicrosparite (L)	
cb245	−6,07	−4,38	SB0015	SCIa	dolomicrosparite (L)	
cb246	−6,31	−4,49	SB0015	SCIa	dolomicrosparite (L)	(loferitic fabric)
cb249	−8,49	−0,13	DOL0021		dolomicrosparite	tectonic stress
cb250	−8,67	−0,16	DOL0021		dolomicrosparite	tectonic stress

Explanations: MAD8122 road outcrop (5 m-thick), MAD8149 road outcrop (5 m-thick), MAD8123 excavation 4 m-thick, MAD8138 road outcrop (4 m-thick), MAD8150 SONOCC quarry (55.6 m thick), MAD0158 cliff (10.6 m-thick), MAD0165 Zonzo hill 60 m-thick, MAD0177 road outcrop (1 m-thick), MAD0183 Loutété River (2.5 m-thick), MAD0184 Kimpendi River (0.5 m-thick), MAD004 hill (19.25 m-thick), MAD0192 road outcrop (0.50 m-thick), MAD0198 River-hill (10 m-thick), MAD202 hill (25 m-thick), MAD0206 road outcrop (6 m-thick), MAD0213 road outcrop (2 m-thick), MAD0220 hill (15 m-thick), MAD0225 road outcrop (2 m-thick), MAD0226 road outcrop (5 m-thick), SB0015 Makoubi quarry (12.7 m-thick, DOL0021 exavation (2 m-thick). NB SCIa = cap carbonate, HCS Hummocky Cross Stratification, (L) Laminar, (S) Speckled on field.

[a] 1 Standard deviation: 0.05% **Sulphates**: pseudomorphs most of the time.

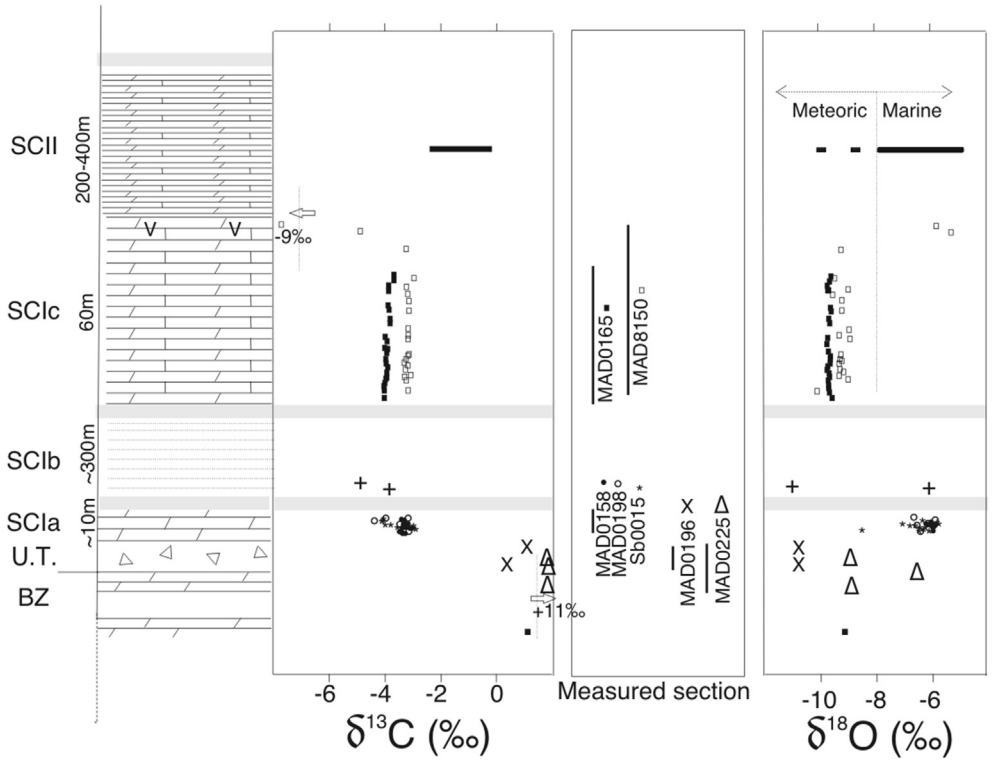

Fig. 14. Composite plots of carbon (left) and oxygen (right) isotope data from all measured sections versus stratigraphic position according to stratigraphic correlation of Dadet (1969). The ordinate axis is an indication of the thickness of the units (see Fig. 3). Abbreviations: BZ = Bouenza Formation, U.T. = Upper Tillite, SC = Schisto-Calcaire, v (in the litholog) = Evaporites. See Table 1 for the list of the sections MAD and Sb0015.

Cailteux et al., 2015; Delpomdor et al., 2015) and our studied area, it appears that the SCI_c overlying the red siltites (of the $SC1_b$) could be coeval with the Nsc1c which overlies the clayey red siltites in SW Gabon and with the C3 Formation in the DRC. Facies change across the basin from SW Gabon with lithoherms (Nsc1c Member *in* Préat et al., 2011) and microbial/evaporitic dolomudstones with ooid/reefal (large stromatolites) packstones/grainstones could be related to the deposition in an actively extending tectonic environment (Tack et al., 2001; Li et al., 2008; Delpomdor and Préat, 2013; Cailteux et al., 2015; Delpomdor et al., 2015).

Recently, Pedrosa-Soares and Alkmin (2011) have proposed six events of rifting and anorogenic magmatism in the area occupied by the Ediacaran Araçuaí-West Congo Orogen (AWCO) and adjacent cratonic domains. Their Cryogenian E6 (750-670 Ga) event is related to oceanic spreading in the central-southern Macaúbas Basin, precursor of the AWCO. These authors indicated that the onset of the pre-collisional magmatic arc in the AWCO has been dated around 630 Ma, with an orogenic climax around 580-570 Ma. Sedimentary features in SW Gabon and the DRC, testify that the first development of carbonate systems along the western margin of the Congo Craton was recorded by alluvial fan system which deepened towards the south and the west, i.e., within the Lower Congo and northern Angolan basins (Delpomdor et al., 2015). In this context, the pre- and post-Marinoan carbonate successions from the DRC are interpreted overall as synrift submarine fan system that was submitted to arid conditions probably occurring by evaporative reflux and humid conditions with inflowing continental freshwater affecting the rift shoulders and upland areas. Our results

demonstrating similar negative $\delta^{13}C$ values in the Cap Carbonates and in the overlying SCI_c carbonates shows that without a detailed timescale for these negative excursions in the lower part of the Schisto-Calcaire Group it may still be a matter of debate.

Strongly heavier $\delta^{18}O$ values (>4‰ from the SCI_c average value) of samples cb91 and cb92 near the top of the SCI_c Member mean that a significant change is to be expected over a short stratigraphic interval (upper part of the SONOCC quarry) submitted to hypersaline brines as highlighted by the abundance of laths of sulphate crystals (mainly anhydrite) possessing a radial arrangement (rosettes). This suggests that near the top of the SCI_c there was no evidence of meteoric waters in the basin and that continental erosion ceased. The low $\delta^{13}C$ values in these two evaporitic carbonate samples could be related to complete oxidation of all organic matter or phytomass in the ocean (Fike et al., 2006). The plot of $\delta^{13}C$ versus $\delta^{18}O$ (Figs. 13 and 14) produces a straight line of sligltly positive slope, its correlation coefficient ($r = 0.40$, $n = 41$) is thought to be due to the diagenetic alteration by the hypersaline fluids as suggested by the sulphate minerals (see microfacies chapter). In more details, the intertidal-supratidal whitish dolomicrosparites with remnants of microbial mats (microbialites) and small-sized LLH-stromatolites (MF7) record the heaviest values ($\delta^{18}O$ −4‰, see Table 2) suggesting evaporation of seawater (Moore, 1989).

Variations of carbon isotopic composition of seawater during the Neoproterozoic, implying repetition of cooling and warming, are difficult to trace because we do not know variations of tectonic forcing (such as volcanic activity) which may affect the carbon cycle and the climate change (Tajika, 2004). It could be argued that the importance of this carbonate pattern for the Cap Carbonates has to be temporized as carbon isotopic compositions of the SCI_c carbonates are the same as those of the Cap Carbonate samples (Fig. 13). According to the discussion above the negative carbon excursion of the SCI_c might be explained by suppression of marine biological productivity in a stagnant equatorial surface ocean during the climate instability, increase in the organic weathering (Tajika, 2004), or related to complete oxidation of all organic matter or phytomass in the ocean (Fike et al., 2006). The second hypothesis (oxidation of organic matter) could be validated as the SCI_c sediments in the Comba Basin were periodically submitted to oxic conditions (ooid shoals). This is also the case with the coeval sediments of the C3 Formation in the Lower Congo Basin where recent chemical analyses (Delpomdor and Préat, 2013; Cailteux et al., 2015; Delpomdor et al., 2015) showed that the sediments belonging to the C3 and C5 formations were deposited in oxic conditions. This might also explain the negative $\delta^{13}C$ values of the Schisto-Calcaire Group in the Comba Basin, e.g., the values being systematically more negative than the ones of the Neoproterozoic oceanic domain (Fig. 14).

Our data concerning a carbonate bed in the clastic Bouenza Formation and two carbonate clasts in the Upper Tillite unit are very poor due to the lack of good exposures. Despite this situation the $\delta^{13}C$ value of the Bouenzian carbonate, Bz_4 unit, (only one sample, MAD0226) gave a very high value (+11.1‰) as the oolitic clasts in the overlying Upper Tillite (Fig. 2). If carbon excursions are driven by global glaciation, the Snowball Earth model predicts positive ^{13}C values in ocean waters prior the onset of glaciation, due to preferential incorporation of ^{12}C in the biomass (synthesis *in* Halverson and Shields-Zhou, 2011). Such positive ^{13}C values (ranging between +2.4‰ and +8.0‰, average + 5.6‰, $n = 20$) have recently been reported in the Lower Congo Basin by Delpomdor et al. (2014) in the uppermost part of the Haut-Shiloango Subgroup, a lateral facies of our studied Bouenza Formation. However, additional study is needed as the carbon (and oxygen) isotopic compositions of two carbonate clasts in the Upper Tillite (MAD0196) gave different values.

Acknowledgements

This study has been supported by Total Exploration & Production Congo in the frame of the National Geological Mapping Program of the Republic of Congo. We are grateful to Total Exploration & Production Congo who supports this program (BRGM/TOTAL E&P CONGO project n°4640001879). This manuscript has benefited from the careful and thoughtful review by François Fournié (University of Aix-Marseille, France).

References

Affaton, P., Kalsbeek, F., Boudzoumou, F., Trompette, R., Thrane, K., Frei, F., 2015. The Pan-African West Congo belt in the Republic of Congo (Congo Brazzaville): stratigraphy of the Mayombe and West Congo supergroups studied by detrital zircon geochronology. Precambrian Res. 272, 185–202.

Allen, P.A., Hoffman, P.F., 2005. Extreme winds and wave in the aftermath of a Neoproterozoic glaciation. Nature 433, 123–127.

Alvarez, Ph, 1992. Répartition de la sédimentation dans le golfe protérozoïque supérieur du Schisto-Calcaire au Congo et Gabon. Implications en Afrique Centrale. Palaeogeogr. Palaeoclimatol. Palaeoecol. 96, 282–297.

Alvarez, Ph, 1995. Evidence for a Neoproterozoic carbonate ramp on the northern edge of the Central African craton: relations with Late Proterozoic intracratonic troughs. Geol. Rundsch. 84, 636–648.

Alvarez, Ph, Maurin, J.C., 1991. Evolution sédimentaire et tectonique du bassin protérozoïque supérieur de Comba (Congo): stratigraphie séquentielle du Supergroupe Ouest-Congolien et modèle d'amortissement sur décrochement dans le contexte de la tectonogenèse panafricaine. Precambrian Res. 50, 137–171.

Alvarez, Ph, Chauvel, J.J., Van Vliet-Lanoë, B., 1995. *Obruchevellla*, cyanobactérie fossile du Protérozoïque supérieur du Congo. Implications sur l'âge du Groupe Schisto-Calcaire et de la glaciation fini-Protérozoïque. Comptes-Rendus Académie Des. Sci. Paris 320 série II a, 639–646.

Arnaud, E., Halverson, G.P., Shields-Zhou, G., 2011. The geological record of Neoproterozoic ice ages. In: Arnaud, E., Halverson, G.P., Shields-Zhou, G. (Eds.), The Geological Record of Neoproterozoic Glaciations. Geological Society of London, Memoir, vol. 36, pp. 1–16.

Béchennec, F., Hutin, G., Martel-Jantin, B., 1981. Cartographie géologique et prospection générale. Mission Nyanga 1980. Région de Tchibanga. Rapport du Bureau de Recherches Géologiques et Minières 81 LIB 004.

Bertrand-Sarfati, J., Vicat, J.P., 1987. Les stromatolites columnaires du Schisto-Calcaire du Protérozoïque supérieur du Congo et leur place dans la sédimentation. Bull. Société géologique Fr. 8 (III, 2), 289–298.

Cahen, L., 1954. Géologie du Congo Belge. Liège, Imprimerie H. Vaillant-Carmanne, S.A., 577 pp.

Cahen, L., Mortelmans, G., 1947. Le système de la Bushimaie au Katanga. Bull. la Société Belge Géologie 56, 217–253.

Cailteux, J.L.H., Delpomdor, F.R.A., Ngoie Ndobani, J.-P., 2015. The Neoproterozoic West-Congo "Schisto-Calcaire" sedimentary succession from the Bas-Congo region (Democratic Republic of the Congo) in the frame of regional tentative correlations. Geol. Belg. 18, 126–146.

Charles, N., Callec, Y., Préat, A., Thiéblemont, D., Delpomdor, F., Malonguila, D., Akouala, A.-P., Ndiele, B., Mvoula Boungou, I., Moebo Boungou, M., 2015a. Carte géologique de la République du Congo à 1/200 000, Feuille Madingou. Editions BRGM.

Charles, N., Callec, Y., Préat, A., Thiéblemont, D., Delpomdor, F., Malounguila, D., Gloaguen, E., Petitot, J., Ackoula, A.-P., Ndiele, B., Mvoula Boungou, I., Moebo Boungou, M., 2015b. Notice explicative de la carte géologique de la République du Congo à 1/200 000, Feuille Madingou. Editions BRGM, 221 pp.

Chorowitz, J., Le Fournier, J., Mvumbi, M.M., 1990. La Cuvette Centrale du Zaïre: un bassin initié au Protérozoïque supérieur. Contribution de l'analyse du réseau hydrographique. Comptes-Rendus l'Académie Sci. Paris 331 (II), 349–356.

Clark, D.N., 1980. The diagenesis of Zechstein carbonate sediments. In: Füchtbauer, H., Peryt, T. (Eds.), The Zechstein Basin with Emphasis on Carbonate Sequences. Stuttgart, E. Schweizerbart'sche Verlagbuchandlung. Contribution to Sedimentology 9, pp. 167–203.

Clough, J.G., Goldhammer, R.K., 2000. Evolution of the Neoproterozoic dolomite ramp complex, Northeastern Brooks range, Alaska. In: Grotzinger, J.P., James, N.P. (Eds.), Carbonate Sedimentation and Diagnesis in the Evolving Precambrian World, vol. 67. Society of Economic Paleontologist and Mineralogists, Special Publication, pp. 209–241.

Dadet, P., 1969. Notice explicative de la carte géologique de la République du Congo-Brazzaville au 1:500.000. Mémoires Bulletin de Recherches Géologiques et Minières, Orléans, France, pp.103.

De Carvalho, H., Tassinari, C., Alves, P.H., Guimarães, F., Simões, M.C., 2000. Geochronological review of the Precambrian in West Angola: links with Brazil. J. Afr. Earth Sci. 31, 383–402.

Delpomdor, F., 2007. Lithostratigraphie et sédimentologie de la chaîne Ouest

Congolienne du Néoprotérozoïque supérieur (Formation de la Diamictite supérieure et Sous-groupe du Schisto-Calcaire) Bas-Congo, République Démocratique du Congo. Unpublished MSc thesis. Université libre de Bruxelles, 138pp.
Delpomdor, F., Préat, A., 2013. Early and late Neoproterozoic C, O and Sr isotope chemostratigraphy in the carbonates of West Congo and Mbuji Mayi supergroups: a preserved marine signature. Palaeogeogr. Palaeoclimatol. Palaeoecol. 389, 35–47.
Delpomdor, F., Préat, A., 2015. Overview of the Neoproterozoic sedimentary series exposed along margins of the Congo Basin. In: De Wit, M.J., Guillocheau, F., de Wit, M.C.J. (Eds.), Geology and Resource Potential of the Congo Basin, Regional Geology Review. Springer Verlag, pp. 41–58.
Delpomdor, F., Kant, F., Préat, A., 2014. Neoproterozoic uppermost Haut-Shiloango Subgroup (West Congo Supergroup, DRC): misinterpreted stromatolites and implications for sea level fluctuations before the onset of the Marinoan glaciation. J. Afr. Earth Sci. 90, 49–63.
Delpomdor, F., Tack, L., Cailteux, J., Préat, A., 2015. The C2 and C3 formations of the Schisto-Calcaire Group (West Congolian Supergroup) in the Democratic Republic of the Congo: an example of Post-Marinoan sea level fluctuations as a result of extensional tectonisms. J. Afr. Earth Sci. 110, 14–33.
Delpomdor, F., Eyles, N., Tack, L., Préat, A., 2016. Pre- and post-Marinoan carbonates facies of the Democratic Republic of the Congo: glacially- or tectonically-influenced deep-water sediments? Palaeogeogr. Palaeoclimatol. Palaeoecolology 457, 144–157.
Dunham, R.J., 1970. Meniscus cement. In: Bricker, O. (Ed.), Carbonate Cements, vol. 19. John Hopkins University Studies in Geology, pp. 297–300.
Esteban, M., Klappa, C.F., 1983. Subaerial exposure environment. In: Scholle, P.A., Bebout, D., Moore, C.H. (Eds.), Carbonate Depostional Environments, American Association of Petroleum Geologists, Memoir, vol. 33, pp. 1–92.
Evans, D.A.D., 2000. Stratigraphic, geochronological, and paleomagnetic constraints upon the Neoproterozoic climatic paradox. Am. J. Sci. 300, 347–433.
Fairchild, I.J., Spiro, B., Herrington, P.M., Song, T., 2000. Control on Sr and C isotope compostions of Neoproterozoic Sr-rich limestones of East Greenland and North China. In: Grotzinger, J.P., James, N.P. (Eds.), Carbonate Sedimentation and Diagnesis in the Evolving Precambrian World, vol. 67. Society of Economic Paleontologist and Mineralogists, Special Publication, pp. 297–313.
Fike, D.A., Grotzinger, J.P., Pratt, L.M., Summons, R.E., 2006. Oxidation of the Ediacaran ocean. Nature 444, 744–747.
Frimmel, H.E., Tack, L., Basei, M.S., Nutman, A.P., Boven, A., 2006. Provenance and chemostratigraphy of the Neoproterozoic West Congolian group in the Democratic Republic of the Congo. J. Afr. Earth Sci. 46, 221–239.
Halverson, G.P., Hoffman, P.F., Schrag, D.P., Maloof, A.C., Rice, A.H., 2005. Toward a Neoproterozoic composite carbon-isotope record. Geol. Soc. Am. Bull. 117, 1181–1207.
Halverson, G.P., Shields-Zhou, G., 2011. Chemostratigraphy and the Neoproterozoic glaciations. In: Arnaud, E., Halverson, G.P., Shields-Zhou, G. (Eds.), The Geological Record of Neoproterozoic Glaciations. Geological Society of London, Memoir, vol. 36, pp. 51–66.
Hardie, L.A., Garett, P., 1977. Some miscellaneous implications and speculations. In: Hardie, L.A. (Ed.), Sedimentation on the Modern Carbonate Tidal Flat of Northwest Andros Island, Bahamas. The John Hopkins Universities Studies in Geology, vol. 22, pp. 184–187.
Hardie, L.A., Ginsburg, R.N., 1977. Layering: the origin and environental significance of lamination and thin bedding. In: Hardie, L.A. (Ed.), Sedimentation on the Modern Carbonate Tidal Flat of Northwest Andros Island, Bahamas. The John Hopkins Universities Studies in Geology, vol. 22, pp. 51–123.
Harris, C.D., Fraunfelter, G.H., 1993. Depositional aspects of Golconda group (Chesterian) oolite bodies, southwestern Illinois Basin. In: Keith, B.D., Zuppann, C.W. (Eds.), Mississippian Oolites and Modern Analogs, American Association Petroleum Geologists, Studies in Geology, vol. 35, pp. 129–140.
Hoffman, P.F., 1974. Shallow and deepwater stromatolites in lower proterozoic facies change, Great Slave lake, Canada. Am. Assoc. Petroleum Geol. Bull. 58, 856–867.
Hoffman, P.F., Kaufman, A.J., Halverson, G.P., Schrag, D.P., 1998. A Neoproterozoic snowball earth. Science 281, 1342–1346.
Hoffman, P.F., Schrag, D.P., 2002. The snowball Earth hypothesis: testing the limit of global change. Terra Nova 14, 129–155.
Hoffman, P.F., Li, Z.X., 2009. A palaeogeographic context for Neoproterozoic glaciation. Palaeogeogr. Palaeoclimatol. Palaeoecolology 277, 158–172.
Inden, R.F., Moore, C.H., 1983. Beach environment. In: Scholle, P.A., Bebout, D., Moore, C.H. (Eds.), Carbonate Depostional Environments, American Association of Petroleum Geologists, Memoir, vol. 33, pp. 211–265.
Jacobsen, S.B., Kaufman, A.J., 1999. The Sr, C and O isotopic evolution of Neoproterozoic seawater. Chem. Geol. 161, 37–57.
Kah, L.C., 2000. Depositional $\delta^{18}O$ signatures in Proterozoic dolostones: constraints on seawater chemistry and early diagenesis. In: Grotzinger, J.P., James, N.P. (Eds.), Carbonate Sedimentation and Diagenesis in the Evolving Precambrian World, vol. 67. Society of Economic Paleontologist and Mineralogists, Special Publication, pp. 345–360.
Kasting, J.F., Howards, M.T., Wallmann, K., Veizer, J., Shields, G., Jaffres, J., 2006. Paleoclimates, ocean depth and the oxygen consumption of seawater. Earth Planet. Sci. Lett. 252, 82–93.
Kennedy, M., Mrofka, D., von der Borch, C., 2008. Snowball Earth termination by destabilization of equatorial permafrost methane clathrate. Nature 459, 642–645.
Kirschvink, J.L., 1992. Late proterozoic low-latitude global glaciation: the snowball earth. In: Schopf, J.W., Klein, C. (Eds.), The Proterozoic Biosphere. Cambridge University Press, pp. 51–52.
Knauth, L.P., Kennedy, M.J., 2009. The late Precambrian greening of the Earth. Nature 460, 728–732.
Land, L.S., 1980. The isotopic and trace element geochemistry of dolomite. In: Zenger, D.H., Dunham, J.B., Ethington, R.L. (Eds.), Concepts and Models of Dolomitization, vol. 28. Society of Economic Paleontologist and Mineralogists, Special Publication, pp. 87–110.
Lepersonne, J., 1974. Carte géologique à l'échelle 1/200.000. Notice explicative de la feuille Ngungu (degré carré S6/14 = SB 33.9). République Démocratique du Congo, Département Mines Direction du Service Géologique, 66 pp.
Logan, B.W., Rezak, R., Ginsburg, R.N., 1964. Classification and environmental significance of algal stromatolites. J. Geol. 72, 6–83.
Li, Z.X., Bogdanova, S.V., Collins, A.S., Davidson, A., De Waele, B., Ernst, B.E., Fitsimons, I.C.W., Fuck, R.A., Gladkochub, D.P., Jacobs, J., Karlstom, K.E., Lu, S., Natapov, L.M., Pease, V., Pisarevsky, S.A., Thrane, K., Vernikovsky, V., 2008. Assembly, configuration, and break-up history of Rodinia: a synthesis. Precambrian Res. 160, 179–210.
Mamet, B., Préat, A., 2005. Sédimentologie de la série viséenne d'Avesnes–sur-Helpe (Avesnois, Nord de la France). Geol. Belg. 81, 91–107.
Master, S., Rainaud, C., Armstrong, R.A., Phillips, D., Robb, L.J., 2005. Provenance ages of the Neoproterozoic Katanga Supergroup (Central African Copperbelt), with implications for basin evolution. J. Afr. Earth Sci. 42, 41–60.
Mickala, O.R., Vidal, L., Boudzoumou, F., Affaton, P., Vandamme, D., Borschnek, D., Mbina Mounguengui, M., Fournier, F., Nganga, D.M., Miche, H., 2014. Geochemical characterization of the Marinoan 'cap carbonate' of the Niari-Nyanga Basin (Central Africa). Precambrian Res. 255, 367–380.
Monié, P., Bosch, D., Bruguier, O., Vauchez, A., Rolland, Y., Nsungani, P., Buta, N.A., 2012. The late Neoproterozoic/early palaeozoic evolution of the West Congo belt of NW Angola: geochronological (UPb and Ar-Ar) and petrostructural constraints. Terra Nova 24 (3), 1–10.
Moore, C.H., 1989. Carbonate Diagenesis and Porosity, vol. 46. Elsevier Science Publishers, USA, Canada, Developments in Sedimentology, 338 pp.
Pedrosa-Soares, A.C., Alkmin, F.F., 2011. How many rifting events preceded the development of the Araçuaí-West Congo orogen? Geonomos 19, 244–251.
Poidevin, J.-L., 1985. Le Protérozoïque supérieur de la République Centrafricaine, Annales du Musée Royal de l'Afrique Centrale, Tervuren, Belgique. Sci. Géologiques 91, 75 pp.
Poidevin, J.-L., Pin, C., 1986. 2 Ga U-Pb zircon dating of Mbi graniodiorite (Central African Republic) and its bearing on the chronology of the Proterozoic of Central Africa. J. Afr. Earth Sci. 5–6, 581–587.
Poidevin, J.L., 2007. Stratigraphie isotopique du strontium et datations des formations carbonatées et glaciogéniques néoprotérozoïques du Nord et de l'Ouest du craton du Congo. Comptes Rendus Géosciences 339, 259–273.
Poidevin, J.-L., Alabert, J., Miauton, J.D., 1981. Géologie des séries du Précambrien supérieur de la région de Bakouma (République Centrafricaine). Bull. du Bureau de Recherches Géologiques Minières, Sect. IV 4, 313–320.
Préat, A., Kolo, K., Prian, J.P., Delpomdor, F., 2010. A peritidal evaporite environment in the Neoproterozoic of south Gabon (Schisto-Calcaire Subgroup, Nyanga Basin). Precambrian Res. 177, 253–265.
Préat, A., Prian, J.P., Thiéblemont, D., Mabicka Obama, D., Delpomdor, F., 2011. Stable isotopes of oxygen and carbon compositions in the Neoproterozoic of South Gabon (Schisto-Calcaire Subgroup, Nyanga Basin): are cap carbonates and lithoherms recording a particular destabilization event after the Marinoan glaciation? J. Afr. Earth Sci. 60, 273–287.
Prian, J.P., Thiéblemont, D., Préat, A., Goujou, J.C., Simo Ndounze, S., Ekogha, H., 2009. Notice explicative de la Carte géologique de la République du Gabon à 1/200 000, feuille Ndendé. Editions DGMG – Ministère des Mines, du Pétrole, des Hydrocarbures, Libreville.
The Persian Gulf. In: Purser, B.H. (Ed.), 1973. Holocene Carbonate Sedimentation and Diagenesis in a Shallow Epicontinental Sea. Springer-Verlag, New York, Berlin, 471 pp.
Purser, B.H., Evans, G., 1973. Regional Sedimentation along the Trucial Coast, SE Persian Gulf. Holocene Carbonate Sedimentation and Diagenesis in a Shallow Epicontinental Sea. Springer-Verlag, New York, Berlin, pp. 211–231.
Reitner, J., Arp, G., Thiel, V., Gautret, P., Galling, U., Michaelis, W., 1997. Organic matter in Great Salt Lake Ooids (Utah, USA) – first approach to a Formation via organic matrices. Facies 36, 210–219.
Scolari, G., 1965. Etude géologique du bassin du Niari oriental (République du Congo-Brazzaville) et ses minéralisations Cu-Pb-Zn. Mémoires du Bureau de Recherches Géologiques et Minières, 35, Paris.
Sellwood, B.W., 1986. Shallow-marine carbonate environments. In: Reading, G.A. (Ed.), Sedimenatry Environments and Facies, second ed. Blackwell Scientific Publications, Oxford, pp. 283–342.
Shields, G.A., 2005. Neoproterozoic cap carbonates: a critical appraisal of existing models and the plumeworld hypothesis. Terra Nova 17, 299–310.
Shukla, V., Friedman, G.M., 1981. An unusual occurrence of surficial anhydrite in a moist temperature zone : example from the Lockport Formation (Middle Silurian) of New York. Sediment. Geol. 29, 125–131.
Straathof, G.B., 2011. Neoproterozoic Low Latitude Glaciations: an African Perspective. Unpublished PhD thesis. University of Edinburgh, 285 pp.
Tack, L., Wingate, M.T.D., Liégeois, J.P., Fernandez-Alonso, M., Deblond, M., 2001. Early Neoproterozoic magmatism (1000-910 Ma) of the Zadinian and Mayumbian groups (Bas-Congo), onset of Rodinia rifting at the western edge of the Congo Craton. Precambrian Res. 110, 277–306.

Tait, J., Delpomdor, F., Préat, A., Tack, L., Straathof, G., Kanda Nkula, V., 2011. Neoproterozoic sequences of the West Congo and Lindi/Ubangi supergroups in the Congo Craton, Central Africa. In: Arnaud, E., Halverson, G.P., Shields-Zhou, G. (Eds.), The Geological Record of Neoproterozoic Glaciations. Geological Society of London, Memoir, vol. 36, pp. 185–194.

Tajika, E., 2004. Analysis of carbon cycle system during the Neoproterozoic: implications for snowball Earth events. In: Jenkins, G.S., McMenamin, M.A.S., McKay, C.P., Sohl, L. (Eds.), The Extreme Proterozoic: Geology, Geochemistry and Climate. International Union of Geodesy and Geophysics vol., Geophysical Monograph, vol. 146, pp. 45–54.

Thiéblemont, D., Castaing, C., Billa, M., Bouton, P., Préat, A., 2009. Notice explicative de la Carte géologique et des Ressources minérales de la République gabonaise à 1/1.000.000. Editions DGMG, Ministère des Mines, du Pétrole, des Hydrocarbures, Libreville, 381pp.

Trompette, R., Boudzoumou, F., 1988. Paleogeographic significance of stromatolitic buildups on late Proterozoic platform: the example of the West Congo basin. Palaeogeogr. Palaeoclimatol. Palaeoecol. 66, 101–112.

Tucker, M.E., Wright, V.P., 1990. Carbonate Sedimentology. Blackwell Scientific Publications, Oxford, 482 pp.

Verbeek, T., 1970. Géologie et lithostratigraphie du Lindien (Précambrien supérieur du nord de la République Démocratique du Congo). Ann. Musée R. l'Afrique Cent. série n°8 66, 309 pp.

Vicat, J.-P., Vellutini, P.-J., 1987. Sur la nature et la signification des dolérites du bassin précambrien de Sembé-Ouesso (République Populaire du Congo). Precambrian Res. 37, 57–69.

Wachter, E., Hayes, J.M., 1985. Exchange of oxygen isotopes in carbon-dioxyde phosphoric acid systems. Chem. Geol. 52, 365–374.

Wagner, C.W., van der Togt, C., 1973. Holocene sediment types and their distribution in the southern Persian Gulf. In: Purser, B.H. (Ed.), Holocene Carbonate Sedimentation and Diagenesis in a Shallow Epicontinental Sea. Springer-Verlag, New York, Berlin, pp. 123–155.

Walemba, K.M.A., Master, S., 2005. Neoproterozoic diamictites from the Itombwe synclinorium, Kivu province, Democratic Republic of the Congo: palaeoclimatic significance and regional correlations. J. Afr. Earth Sci. 42, 200–210.

Wendorff, M., Key, R.M., 2009. The relevance of the sedimentary history of the Grand Conglomérat Formation (Central Africa) to the interpretation of the climate during a major Cryogenian glacial event. Precambrian Res. 172, 127–142.